The LINC complex component Kms1 and CENP-B protein Cbp1 cooperate to enforce faithful homology-directed DNA repair at the nuclear periphery in *S. pombe*

Alyssa Laffitte[1], Dongxu Lin[1], Yingzhen Jenny Tian[2,3], Na Liu[1], C. Patrick Lusk[1], Simon G. J. Mochrie[2,4], and Megan C. King[1,5*]

1 Department of Cell Biology, Yale School of Medicine, New Haven, CT, USA, 06520
2 Department of Physics, Yale University, New Haven, CT, USA, 06510
3 Integrated Graduate Program in Physical Engineering Biology, Yale University, New Haven, CT, USA, 06510
4 Department of Applied Physics, Yale University, New Haven, CT, USA, 06510
5 Department of Molecular, Cell, and Developmental Biology, Yale University, New Haven, CT, USA, 06510
*To whom correspondence should be addressed: megan.king@yale.edu

Abstract

While homologous recombination (HR) is often considered to be an error-free DNA repair mechanism in mitotically growing cells, the ultimate fidelity of this pathway depends on the cell's ability to engage the ideal template, the replicated sister chromatid. This is particularly challenging during repair of repetitive regions of the genome for which non-allelic sequences can errantly be used as templates. Here, we develop a model to study spontaneous DNA damage and repair that occurs at repetitive protein coding genes of the *S. pombe* flocculin family. We observe that the genes encoding most members of this protein family constitutively reside at the nuclear periphery by virtue of their close proximity to binding sites for the CENP-B like protein, Cbp1. Tethering via Cbp1 to the nuclear periphery enhances the stability of the flocculin genes against intragenic recombination and restrains intergenic recombination between homeologous repeat-encoding sequences. In addition, the LINC complex component Kms1, which we have previously shown associates with persistent DNA double-strand breaks that move to the nuclear periphery, also antagonizes both intragenic and intergenic recombination at the flocculin genes. Loss of Kms1 also enhances use of microhomology-mediated end-joining (MMEJ). Our observations suggest that *S. pombe* leverages nuclear compartmentalization to maintain the stability of repetitive genic regions through a constitutive tethering mechanism at the nuclear periphery. Moreover, association of DSBs with Kms1-containing LINC complexes enforces stringency to both attenuate the use of microhomology that drives mutagenic end-joining or selecting the correct template for HR.

Introduction

DNA double-stranded breaks (DSBs) are the most toxic type of DNA damage. Failure to efficiently and accurately repair DSBs can lead to mutations, gross chromosomal rearrangements, and cell death (Cannan & Pederson, 2016). Cells use two major pathways to repair DSBs: canonical non-homologous end-joining (cNHEJ) and homologous recombination (HR). cNHEJ, the pathway of choice in the G1 phase of the cell cycle (Hustedt & Durocher, 2016), involves the direct ligation of the broken DNA ends. In general, cNHEJ is promoted by the DSB end-binding Ku70/80 complex and DNA ligases, most canonically Lig4 in eukaryotes (Sallmyr et al., 2024). While so-called "clean" DSB ends are efficiently ligated by Lig4, so-called "dirty" DSBs that contain blocking chemical adducts must be further processed prior to ligation (Biehs et al., 2017; Ellenberger & Tomkinson, 2008; Jeggo & and Lobrich, 2005; Sasanuma et al., 2020; Schipler & Iliakis, 2013). In either case, the repair products of cNHEJ often contain small insertions and deletions. In contrast, homologous recombination (HR) is up-regulated in the S and G2 phases of the cell cycle and represents a virtually error-free DSB repair pathway that engages the sister chromatid as a template for new DNA synthesis (Branzei & Foiani, 2008; Haber, 2018; Krejci et al., 2012; Li & Heyer, 2008; Lu et al., 2017). In order to achieve this, HR requires the resection of the 5' ends of the DSB, creating 3' single-stranded overhangs; these unstable ssDNA overhangs are protected by rapid recruitment of the abundant, ssDNA-binding Replication Protein A (RPA) complex (Symington, 2016). In yeasts, including the fission yeast *S. pombe*, further recruitment of Rad52 facilitates remodeling to load the recombinase Rad51, generating the nucleoprotein filament (New et al., 1998), which in turn catalyzes the search for the homologous sister chromatid to use as a template for new synthesis (McIlwraith & West, 2008). Although it is challenging to monitor, the prevalent DSB repair mechanism in mitotically growing *S. pombe* cells, which reside primarily in the G2 phase of the cell cycle, is likely synthesis-dependent strand annealing (SDSA), a non-crossover form of HR (Elbakry & Löbrich, 2021; Haber, 2018; Helleday et al., 2007; Li & Heyer, 2008; Vines et al., 2022).

Due to its high fidelity, HR is considered the preferred pathway when the sister chromatid is available. However, the fidelity of the HR repair product depends on the cell's ability to identify the correct homologous sequence to use as a template. Following DNA synthesis, the sister chromatids are tethered together by replicative cohesin complexes, limiting the need for an extensive homology search for productive, allelic HR as it likely enhancing use of the correct template. Cohesin's role in loop extrusion may also contribute to the homology search (Covo et al., 2010; Dumont et al., 2024; Piazza et al., 2021). However, faithful repair of tandem repeats nonetheless presents a challenging problem for the cell, including increasing the rate of replication fork stalling (Polleys et al., 2017; Triplett et al., 2024). During HR, strand invasion into a like repeat can drive intramolecular gene conversion or unequal sister chromatid exchanges if a cross-over occurs, driving repeat copy number changes (Hastings et al., 2009); SDSA (a non-crossover repair mechanism) can likewise lead to changes in repeat copy number (Elbakry & Löbrich, 2021; Wright et al., 2018). Use of an illegitimate repair templates at other genomic sites can be even more deleterious, leading to large deletions, insertions, loss-of-heterozygosity, or chromosomal translocations (Nian et al., 2024). However, for such repair outcomes to occur, the DSB must come into physical proximity with these non-allelic sequences (Renkawitz et al., 2014; Wang et al., 2017).

A key mechanism that eukaryotic cells employ to protect repetitive regions from aberrant recombination leverages nuclear compartmentalization. In most biological contexts, the compartment at the nuclear periphery is enriched in both repetitive and silenced DNA, which are highly correlated (Padeken & Heun, 2014; Padeken et al., 2022); this relationship is often suggested to reflect heterochromatization of repetitive foreign DNA elements such as transposons including in fission yeast (Marsano & Dimitri, 2022; Murton et al., 2016; Padeken et al., 2022). However, in yeast models, including *S. cerevisiae* and *S. pombe*, there is also the observation that some actively expressed, multi-copy genes also reside at the nuclear periphery, suggesting that these two facets could be uncoupled (Ahmed et al., 2010; Ahmed & Brickner, 2007; Brickner & Walter, 2004; Casolari et al., 2004; Chen & Gartenberg, 2014; Matsuda et al., 2017; Steglich et al., 2013; Sumner & Brickner, 2022). The best investigated examples are Pol III encoded genes such as tRNA genes and the 5S RNA genes (in *S. pombe*) that cluster in 3D space in the nucleus at the nuclear periphery (and on the nucleolar surface) that have been referred to as "TFIIIIC bodies" (Cam et al., 2008; Chen & Gartenberg, 2014; Gallardo et al., 2019; Iwasaki et al., 2010; Lorenz et al., 2012). Indeed, the concept that the compartment of the nuclear periphery is compatible with productive gene expression is highlighted by a body of literature tying the movement of highly expressed genes to nuclear pore complexes (NPCs) (Ahmed et al., 2010; Ahmed & Brickner, 2007; Brickner & Walter, 2004; Matsuda et al., 2017; Steglich et al., 2013; Sumner & Brickner, 2022). Thus, considering the nuclear periphery as a single compartment may be overly simplistic, consistent with differential roles for the integral inner nuclear membrane proteins including Heh1/Lem2, and Mps3/Sad1 and the NPC in orchestrating faithful DNA repair (Capella et al., 2021; Churikov et al., 2016; Conrad et al., 2008; Horigome et al., 2016; Horigome et al., 2014; Kalocsay et al., 2009; Kramarz et al., 2020; Moser et al., 2020; Nagai et al., 2008; Oza et al., 2009; Ryu et al., 2015)

With regards to the mechanisms enforcing genomic stability, across model systems a key observation is that pro-recombination factors are inhibited from loading within the repeat-rich domain, with DSBs physically moving outside of the domain before HR proceeds; conceptually such a mechanism would help ensure use of the sister chromatid as a template HR rather than other repeats co-localized in the nuclear "neighborhood" of the DSB (Amaral et al., 2017; Anand et al., 2014; Caridi et al., 2017; Choi et al., 2022; Merigliano & Chiolo, 2021; Wang et al., 2017). For example, in budding yeast a DSB in the rDNA repeats fails to recruit Rad52 until the lesion moves outside of the nucleolus, permitting HR to proceed (Torres-Rosell et al., 2007). In *Drosophila*, DSBs induced by irradiation within heterochromatin similarly fail to load Rad51; here, heterochromatic histone modifications and their binding proteins, well-known to be enriched at repetitive genome regions, are necessary for this regulation (Chiolo et al., 2011). In line with this model, the recruitment of HR factors is disfavored at DSBs associated with the nuclear lamina in mammalian cells (Lemaître et al., 2014). Moreover, DSBs in pericentric heterochromatin in human cells must move out of the heterochromatic domain in order to productively load Rad51 after replication, while DSBs at centromeric heterochromatin are positionally stable and recruit Rad51 and RPA throughout the cell cycle (Tsouroula et al., 2016). Taken together, these studies suggest conserved mechanisms by which repetitive regions of the genome are subject to additional controls over DSB repair by HR.

Given the roles for nuclear position and/or chromatin state in impacting HR outcomes, restricting or enhancing the mobility of DSBs in or out of nuclear subcompartments can also play a role. The Smc5-Smc6 complex and its ability to engage the SUMOylation machinery appears key to the regulation of DSB repair in repeat-rich domains. Defects in Smc5-6 can both lead to aberrant loading of pro-HR factors in repeat-rich domains and disrupts the movement of the DSB outside of the domain, leading to heightened repeat instability in budding yeast and *Drosophila* (Chiolo et al., 2011; Torres-Rosell et al., 2005; Tsouroula et al., 2016). Additionally, in human cells, Smc5 has been shown to localize to the nucleolus after induction of a DSB within the rDNA, and loss of Smc5 caused a reduction BRCA1 and Rad51 recruitment to these lesions (Warmerdam et al., 2016), suggesting that Smc5 is involved in the repair of repetitive regions of DNA by the HR pathway. SUMOylation is also tied to the movement of persistent DSBs to the nuclear periphery when their repair is inefficient, even when they arise in euchromatic regions of the genome normally residing in the nuclear interior. For example, irreparable DSBs associate with NPCs, where the associated SUMO E3 ubiquitin ligase Slx5-Slx8 complex is thought to help promote HR (Churikov et al., 2016; Horigome et al., 2016; Kalocsay et al., 2009; Ryu et al., 2015). The NPC proteins Nup84 and Slx8 are also involved in resolving DNA damage at collapsed replication forks, as loss of these proteins causes an increase in spontaneous gene conversion events (Nagai et al., 2008; Whalen et al., 2020). Fission yeast likewise execute similar mechanisms, although they have been less studied to date. In *S. pombe* the E3 SUMO ligase Pli1 acts at stalled replication forks to pause DNA synthesis and promotes relocation of the DSB to the NPC; once arriving at the NPC, SUMO is removed, allowing DNA synthesis to resume (Kramarz et al., 2020).

The Linker of Nucleoskeleton and Cytoskeleton (LINC) complexes and their constituent SUN and KASH domain proteins at the nuclear envelope appear to play a distinct role in regulating DSB repair. We previously demonstrated that persistent DSBs captured at the nuclear periphery by association with the SUN domain protein, Sad1, could engage with the KASH domain protein, Kms1, in the outer nuclear membrane to form a LINC complex that coupled the DSB to dynamic cytoplasmic microtubules (Swartz, 2014). In line with these results, previous work in budding yeast revealed that mutation of the nucleoplasmic domain of the SUN domain protein Mps3 disrupted recruitment of DSBs to the nuclear periphery while slowly-repairing DSBs were likely to be targeted to the nuclear periphery where they bound to Mps3 (Oza et al., 2009). Similar complexes and their ability to influence DSB repair have subsequently been broadly observed across eukaryotic models (Lawrence et al., 2016; Lottersberger et al., 2015). Interestingly, while we observed that Kms1 promoted a long-range homology search required for a templated, interhomologue-like repair event, Kms1 also appeared to antagonize a poorly understood repair mechanism that allowed HR-deficient (*rad51Δ*) cells to survive (Swartz, 2014). One limitation of this study, like many, was that it primarily relied on the study of an inducible DSB that is irreparable in haploid cells, calling into question whether the observations reflect events those that occur at naturally occurring DSBs that can be repaired using the sister chromatid as a template.

Taken together, a model is emerging in which early steps in HR, including resection, can occur at DSBs in repeat-rich compartments (Chen & Tyler, 2022; van Bueren & Janssen, 2024). However, HR is then stalled in repeat-rich domains, an effect requiring SUMOylation, which also likely facilitates movement of the DSB outside of the domain. At least in part, factors at the

NPC likely act to relieve this inhibition to allow HR to proceed, thereby preserving genome integrity. While such regulation appears to act constitutively in repetitive and/or heterochromatic regions of the genome, it is also triggered more generally when DSB repair is inefficient. Association of DSBs with SUN domain proteins and/or LINC complexes also influences the outcomes of repair, either by impacting the modulation of the SUMO to ubiquitin relay at the NPC and/or by physically influencing either the localization or dynamics of the DSB in the nucleus (Lawrence et al., 2016; Lottersberger et al., 2015; Swartz, 2014; Wong et al., 2021). One challenge to disentangling the mechanisms that are imparted by nuclear position versus chromatin state is the strong relationship between repetitive DNA and heterochromatin. One approach to investigating mechanisms impacting repeat stability independent of heterochromatin is to monitor the mechanisms that stabilize expressed protein coding genes that are intrinsically repetitive at the DNA and protein sequence level.

Here, we develop a model to study spontaneous DNA damage and repair that occurs within a family of protein repeat-containing genes that encode *S. pombe* flocculins. We observe that the genes encoding most members of this protein family reside at the nuclear periphery, which we tie to nearby binding sites for the CENP-B like protein, Cbp1/Abp1. Tethering via Cbp1 to the nuclear periphery enhances the stability of the flocculin genes to both intragenic recombination within the protein repeat-encoding sequence and restrains intergenic recombination between homeologous repeat-encoding sequences. In addition to the constitutive tethering of the flocculin genes to the nuclear periphery by Cbp1, the LINC complex component Kms1 appears to play a distinct role in enforcing genome stability. Using an assay to study alternative or “salvage” DNA repair mechanisms, we found that Kms1 restrains the use of microhomology-mediated end-joining (MMEJ), a mutagenic salvage DNA repair pathway. Taken together, our findings suggest a model in which Cbp1 and Kms1 both act to promote the stability of repetitive regions of the genome.

Results

S. pombe flocculin-like (*pfl*) genes are repetitive and localize to the nuclear periphery.

To investigate the mechanisms that promote genome stability of euchromatic, repetitive sequences, we sought to identify protein-coding genes containing internal repeats. We hypothesized that the *S. pombe* flocculin-like genes (*pfl*s), a rapidly evolving, expressed family of proteins (Fig. 1A and Supplemental Fig. 1) targeted to the cell surface that mediate cell-cell and cell-environment interactions (Kwon et al., 2012) could serve as such a model. Like the FLO genes of *S. cerevisiae* (also called adhesins) that are responsible for flocculation, biofilm formation and pseudohyphae (Verstrepen & Klis, 2006) the *pfl* genes encode similar structures that include a signal sequence, a variable number of highly related repeats of 35-36 amino acids (~100 base pairs) and a ligand binding domain predominantly from one of two family – GLEYA and DIPSY (Linder & Gustafsson, 2008) (Fig. 1A, Supplemental Fig. 2). As the nuclear periphery has been broadly observed to stabilize repetitive regions of the genome, we first explored the subnuclear position of the *pfl* genes.

To achieve this, we turned to the lacO/lacI-GFP chromatin tagging system to assess the location of *pfl* gene loci within the nuclear volume. We inserted a lacO array adjacent to the following *pfl* gene loci: *pfl*5, *pfl*10, and *pfl*3 and the mating adhesin genes in the *pfl* family, *mam3* and *map4* (Mata & Bähler, 2006; Sharifmoghadam et al., 2006). As a comparison, we leveraged a euchromatic, non-*pfl* locus on the arm of chromosome II that we characterized previously (*cut3*)(Zhao et al., 2016). To visualize the lacO array we expressed a tetramerization-deficient version of lacI fused to GFP and a nuclear localization signal, while we reconstruct the contour of the nuclear envelope based on the nucleoporin Cut11 as an mCherry fusion, as in our prior work (Zhao et al., 2016). After acquiring z-stacks of both signals we employed custom MatLab image analysis pipelines we developed previously to fit the lacO/lacI-GFP signal to a Gaussian described by the point spread function and to reconstruct the nuclear surface (Zhao et al., 2016). In line with our prior observations, *cut3* was typically located within the nuclear interior, as illustrated by the representative cell and reconstruction in Fig. 1B. To assess populations of cells, we plotted the probability distribution of distances from the center of the lacO/lacI-GFP Gaussian to the nearest point of the nuclear contour (normalized for nuclear size). Using this approach, we observed that *cut3* has a nearly uniform distribution throughout the nucleoplasm (Fig. 1C, pink). In comparison, *pfl*5 was found to be associated with the nuclear periphery as shown in the representative reconstruction in Fig. 1D and enriched at the nuclear periphery and depleted from the nuclear interior across a population of cells (Fig. 1C, brown). We observe a similar preference for a peripheral nuclear position for *map4* and *mam3* (Fig. 1E and Supplemental Fig. 3). While *pfl10* and *pfl3* did not show the same extent of enrichment as *pfl5* at the nuclear periphery, they are nonetheless depleted from the interior of the nucleus compared to *cut3* (Fig. 1E and Supplemental Fig. 3). Given their preferential association with the nuclear periphery, we employed the *pfl* gene family to further explore the relationship between nuclear position and the stability of repetitive protein-coding genes.

1

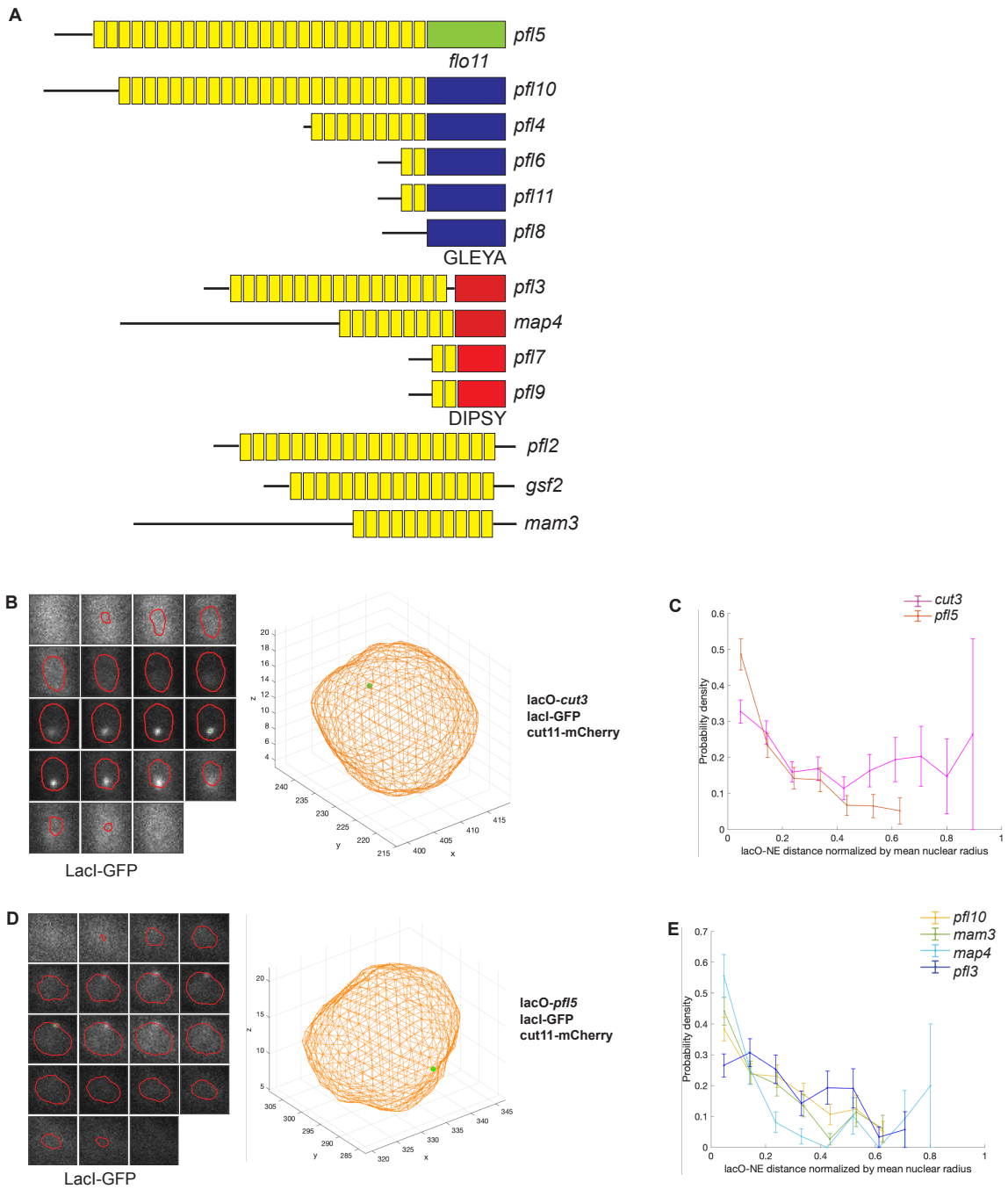

Figure 1. *S. pombe* flocculin-like (*pfl*) genes are a family of repetitive genes that localize to the nuclear periphery. A) *Pfl* genes encode similar structures that include a signal sequence (black line), a variable number of related repeats (yellow rectangles), and a ligand binding domain from one of two families: GLEYA (dark blue rectangles) and DIPSY (red rectangles). B) We use a lacO/lacI-GFP system to visualize the location of each *pfl* gene within the nuclear volume. A series of lacO repeats was inserted at the generic locus *cut3*, and at *pfl5*, in strains expressing a Cut11-mCherry fusion (not shown). Collecting multiple z-stacks of both signals allowed us to create a 3D reconstruction of the nucleus. Here, the lacO at *cut3* is centrally located within the nucleus. C) A probability density analysis shows that the lacO at *pfl5* is enriched at the nuclear periphery and depleted from the nuclear interior, while the lacO at *cut3* is broadly distributed across the nucleoplasm. D) A representative 3D reconstruction showing the lacO at *pfl5* at the nuclear periphery. E) A probability density analysis shows that the position of the lacO at each *pfl* gene tested (*pfl10, mam3, map4, and pfl3*) is biased towards the nuclear periphery.

Proteins involved in homologous recombination enforce stability of *pfl* genes

Given that direct repeats are prone to genetic instability due to intragenic recombination (Novarina et al., 2020; Rudin et al., 1989; Smith & Rothstein, 1999), we next asked if the *pfl* genes are likewise prone to genetic instability. To assess this, we inserted a copy of the *ura4* gene within the direct repeats encoded by members of the *pfl* family (Fig. 2A). Cells were maintained on minimal medium without uracil before being subjected to fluctuation tests. To measure the stability of each *pfl* gene, cultures were inoculated into rich medium to allow for survival of cells that lost functional *ura4*. After saturation was achieved by 24 hours of growth in rich medium, the culture was plated to 5-Fluoorotic acid (5-FOA, a drug that produces a toxic metabolite in *ura4*+ cells) to select for cells that had undergone spontaneous loss of *ura4* from the following *pfl* genes: *pfl3*, *pfl5*, *pfl10*, *mam3*, and *map4*. Counting the colonies that grew on 5-FOA relative to all cells plated (assessed from parallel plating on YE5S) allowed us to measure the rate of loss of *ura4* (Table 1). Given the range of direct repeat number inherent to the *pfl* gene family (Fig. 1A), we first asked if and how intrinsic instability is related to the number of repeats; a positive correlation was previously described between repeat copy number and intrinsic instability for the flocculin genes of *S. cerevisiae* (Verstrepen & Klis, 2006). As in this prior study, we observed a positive correlation between the frequency of 5-FOA-resistant colonies and repeat number (r^2=0.8117), with *pfl5* (with 26 direct repeats) and *pfl10* (with 24 direct repeats) showing the highest rates of colony formation on 5-FOA (1.53×10^{-5} and 1.41×10^{-5}, respectively) while *map4* and *mam3* with 9 and 10 direct repeats, respectively, showed the lowest rates of colony formation (1.59×10^{-6} and 5.25×10^{-6}) (Fig. 2B). Importantly, the rate of spontaneous inactivating mutations in *ura4* at its endogenous locus are over three orders of magnitude less prevalent ($<1 \times 10^{-8}$)(Pai et al., 2023). Our tests to measure the rate of loss of endogenous *ura4* yielded similar results.

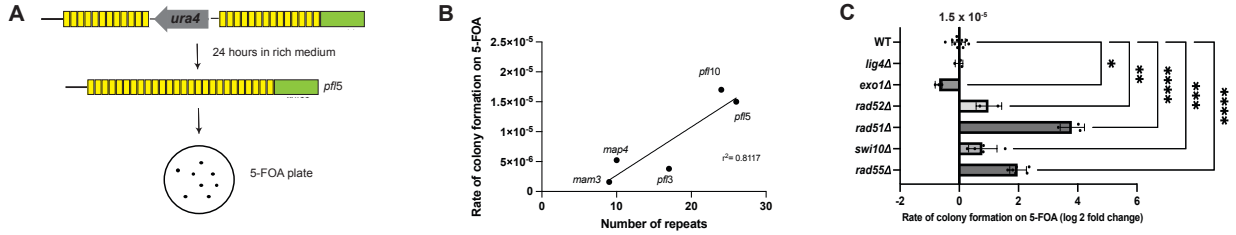

Figure 2. *Pfl* genes are genetically unstable. A) To measure the stability of repetitive regions of *pfl* genes, we inserted a *ura4* into the direct repeats within the *pfl* genes (represented by *pfl*5 here). Releasing the cells into rich medium allowed survival of cells that had undergone recombination and thus, lost functional *ura4*. Plating to 5-FOA and counting the colonies that formed relative to total colony number on rich media allowed us to calculate the frequency of recombination within this region. B) Across *pfl* loci, repeat number correlates with the rate of recombination (r^2= 0.8117). C) HR-related DNA repair mechanisms (rather than cNHEJ) impact the rate of *ura4* loss at *pfl*5. Loss of Lig4 shows no effect on the rate of loss of *ura4*. Loss of Exo1 led to a decrease in recombination (p=0.0122 by one-way ANOVA with Dunnett correction for multiple comparisons). Loss of proteins that are involved in SSA or in the recombination step of HR, such as Rad52, Rad51, Rad55, and Swi10, cause a marked increase in the rate of recombination (p=0.0010, p<0.0001, p<0.0001, and p=0.0002, respectively). Data points are the natural log of the fold change in rate.

To provide insight into the mechanism(s) that drive the loss of *ura4* from within the *pfl* genes, we further investigated how disrupting a variety of established DNA repair factors influenced the rate of 5-FOA-resistant colony formation within *pfl5* (Fig. 2C). We examined genetic knockouts of Lig4 (the ligase driving canonical NHEJ), Exo1 (the exonuclease that drives long-range 3'

DSB resection upstream of homology-directed repair in fission yeast (Langerak et al., 2011; Leland et al., 2018), the pro-HR factors Rad52 and Rad51, and Swi10 (the ERCC1 ortholog that promotes single-strand annealing between homologous DNA repeats (Zhang et al., 2014)). The *lig4Δ* strain behaved like WT, consistent with the preference of *S. pombe* to use HR during log phase growth (Ferreira & Cooper, 2004). Loss of Exo1 led to a ~50% decrease in colony formation on 5-FOA, consistent with a role for long-range DSB resection upstream of homology-directed repair leading to loss of *ura4*. Somewhat surprisingly, loss of Rad52, which has roles in both loading of Rad51 onto resected DNA tails to drive HR as well in promoting single-strand annealing (SSA) of RPA-coated ssDNA (New et al., 1998), led to a nearly 3-fold increase in *ura4* instability. Loss of *rad51* itself led to an over 40-fold increase in rates of *ura4* loss. Loss of *rad55* had a similar effect. It is important to note, however, that loss of RAD51 loading also leads to extensive degradation of resected ssDNA (Berti et al., 2020; Bonilla et al., 2020; Hashimoto et al., 2010); caution must therefore be exercised in assuming that this increase in rate reflects that homology-directed repair and/or SSA do not contribute to recombination events leading to loss of the *ura4* sequence in WT cells. Last, we observe that loss of Swi10 led to an increase in colony formation on 5-FOA; given that its orthologs Rad10 (*S. cerevisiae*) and ERCC1 (human cells) have roles in flap cleavage to promote SSA (Osman et al., 2005), this suggests that either 1) despite *ura4* being embedded in direct repeats, this activity is not required, or 2) recombination promoted by Rad51 dominates in WT *S. pombe* in this context.

A subset of *pfl* genes are tethered to the nuclear periphery via the CENP B-like protein, Cbp1

We next considered how the genomic context in which *pfl* genes reside might hint at the mechanism by which most *pfl* genes associate with the nuclear periphery. Like many rapidly evolving gene families, several of the *pfl* genes reside in larger, multicopy segments in the subtelomeric regions of the genome (*pfl*5, *pfl*6, *pfl*7, *pfl*8, *pfl*9, *pfl*11; Fig. 3A); as telomeres are compartmentalized at the nuclear periphery in *S. pombe* (Matsuda et al., 2017), this could restrain their subnuclear position. While this could explain the observation that *pfl*5 localizes close to the nuclear periphery, the other *pfl* genes we characterized are located within the chromosome arms, including *pfl*3, *pfl*10, *map4*, and *mam3*, suggesting an additional mechanism at play. We were intrigued that the genes encoding *pfl*5 and *pfl*10 are directly adjacent to one of the eleven full *Tf2* transposons in *S. pombe* (Fig. 3A). *Tf2* transposons are bound by the CENP-B homologs in fission yeast (Feng et al., 2012), which collectively recruit histone deacetylases to induce their repression (Lorenz et al., 2012); this activity is tied to physical clustering of *Tf2* transposons in "Tf bodies" (Feng et al., 2012). The CENP-B protein Cbp1/Abp1 also associates with abundant long terminal repeats (LTRs) lacking full transposon sequences and can silence nearby genes (Noma et al., 2004), regulate replication fork stability (Zaratiegui et al., 2011), and possibly more generally regulate regions of repetitive sequence (Daulny et al., 2016). We therefore leveraged existing data sets of Cbp1 binding peaks (Daulny et al., 2016) and of histone marks (DeGennaro et al., 2013; Dong et al., 2020) in the *S. pombe* genome to probe for a relationship with *pfl* genes. We first confirmed that a Cbp1 binding peak is found within 600bps of all *Tf2*/LTRs as expected (264/282 or 93.6%) while a baseline prevalence for proximity within 600 bps of all protein-coding genes was 22.6% (1156/5123), likely reflecting the compactness of the *S. pombe* genome (Fig. 3B). Compared to this threshold, Cbp1 peaks were strongly over-represented within 600bps of the *pfl* genes (9/11; 81.8%). More specifically, previously collected ChIP-Seq data demonstrate that the *pfl*3, *pfl*5, and *pfl*10 loci all neighbor at least one Cbp1

binding peak (Fig. 3C) (Daulny et al., 2016; DeGennaro et al., 2013; Dong et al., 2020). Of note, despite its repetitive nature, all three of these *pfl* genes appear at most weakly heterochromatized as assessed by the modest level of the repressive histone mark H3K9me2 and prevalent level of the active histone mark H3K4me3 (Fig. 3C), consistent with their robust gene expression (Supplemental Fig. 1). In the cases of *pfl*5 and *pfl*10, the Cbp1 binding sites are nearby full *Tf2* retrotransposons, *Tf2-11* and *Tf2-3*, respectively (Fig. 3C). The *pfl*10 locus also neighbors multiple Cbp1 binding peaks (Fig. 3C).

Given Cbp1's ability to cluster *Tf2* transposons (Daulny et al., 2016; Murton et al., 2016), and the established relationship between transposable elements and the nuclear periphery (Marsano & Dimitri, 2022; Murton et al., 2016; Padeken et al., 2022), we next tested whether Cbp1 contributes to the tethering of *pfl* genes to the nuclear periphery. We compared the distribution of *pfl5*, *pfl10*, and *pfl3* (one representative of each family within the *pfl* genes) in WT and *cbp1Δ* genetic backgrounds using the lacO/lacI-GFP system (Fig. 4). We observed the clearest effect of the *cbp1Δ* condition on *pfl5*, where it was qualitatively obvious that in many cells the lacO at *pfl5* was more centrally positioned in the nucleus compared to the WT control (Fig. 4A) as reinforced by representative reconstructions (Fig. 4B). Morever, the probability distribution for the lacO at *pfl5* is strongly influenced by deletion of Cbp1 with a loss of enrichment at the nuclear periphery (Fig. 4C). While less dramatic for *pfl3* (Fig. 4D) and *pfl10* (Fig. 4E), both of these loci also became more randomly distributed throughout the nucleoplasm in cells lacking Cbp1. These results suggest that Cbp1 contributes to the peripheral tethering of at least a subset of the *pfl* genes.

1

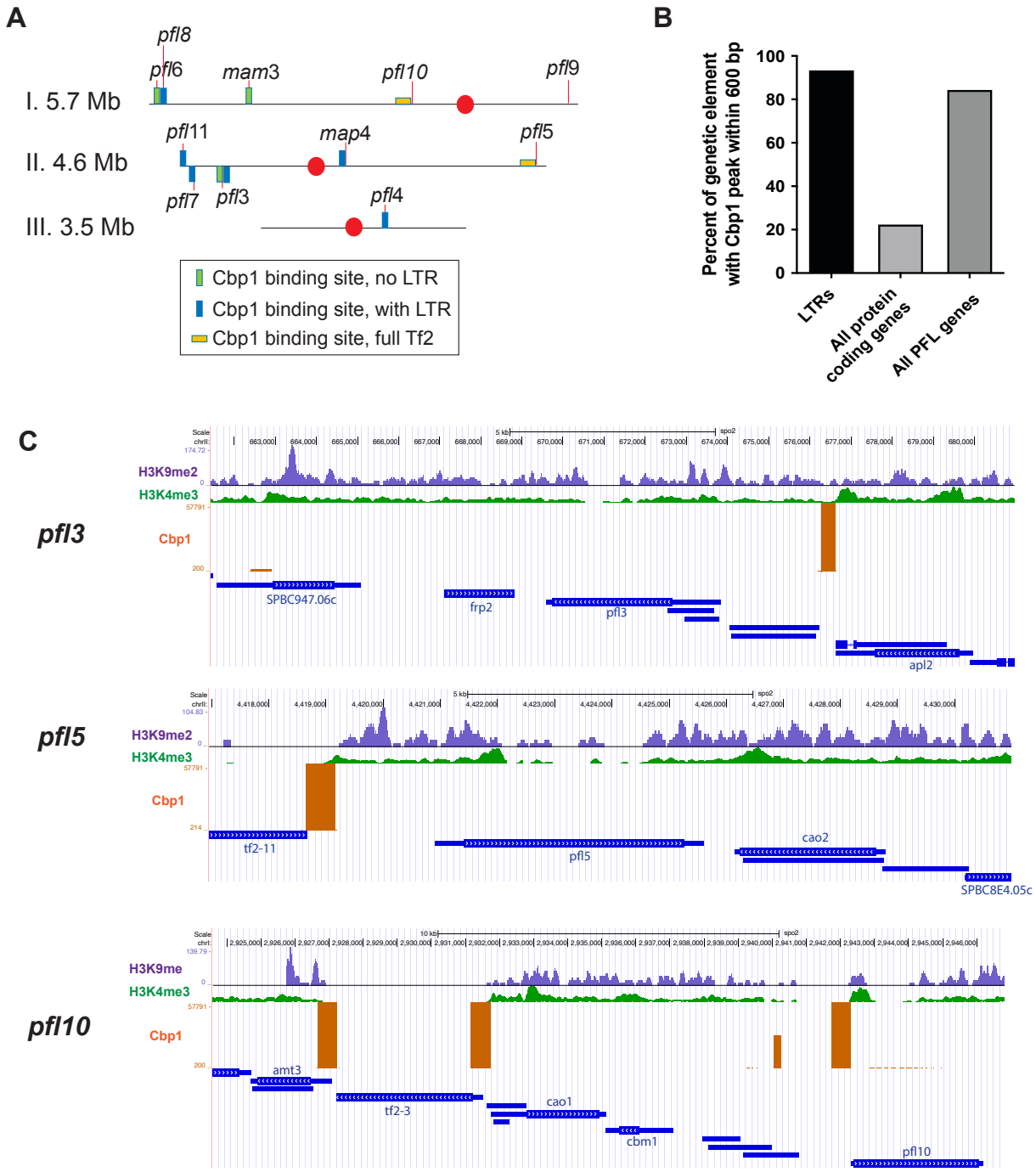

2
3
4

Figure 3. *Pfl* genes are nearby bindings sites for the CENP-B like protein, Cbp1. A) A map of all three chromosomes of *S. pombe*, showing that 91% *pfl* genes are located nearby a Cbp1 binding site. Centromeres are represented by a red dot. B) 91% of LTR retrotransposons show a Cbp1 peak within 600bp, while only 20% of all protein coding genes show a *cbp1* peak within 600bp. All *pfl* genes are more similar to LTRs. C) Existing ChIP-Seq data (Daulny et al., 2016) shows Cbp1 peaks nearby *pfl3, pfl5, and pfl10*. Data for histone marks H3K9me2 and H3K4me3 (DeGennaro et al., 2013; Dong et al., 2020) suggest the loci are actively transcribed.

Cbp1 maintains the stability of *pfl* genes

Cbp1 was previously demonstrated to restrain the recombination of a *Tf1* transgene into remnant *Tf1* LTRs in the *S. pombe* genome (Feng et al., 2012). This finding, in addition to our observation that Cbp1 contributes to the tethering of *pfl* genes to the nuclear periphery, led us to ask if Cbp1 also influences the stability of the *pfl* genes. We again leveraged the intragenic recombination assay to measure the role of Cbp1 and its major binding sites adjacent to its corresponding *pfl* gene. For these experiments, we again focused on *pfl*5, *pfl*3, and *pfl10*, one to represent each *pfl* gene family. Genetic deletion of Cbp1 increased the rate of recombination at both *pfl*5 and *pfl*3 (Figs. 4F-G and Table 1); for *pfl*5 the rate of recombination increased from 1.53×10^{-5} in the WT cells to 5.06×10^{-5} in the *cbp1Δ* cells while for *pfl3* the rate of recombination increased from 4.39×10^{-6} in WT cells to 1.14×10^{-5} in the *cbp1Δ* cells. By contrast, we found that genetic deletion of Cbp1 did not affect genomic stability at *pfl10* (Fig. 4, Table 1). However, deleting the nearby binding site for CENP-B proteins (an intact *Tf2* transposon, *Tf2-3*) caused a two-fold increase in the rate of growth on 5-FOA (Fig. 4H and Table 1). These observations support the hypothesis that tethering to the nuclear periphery through Cbp1 for *pfl5* and *pfl3*, and possibly in concert with other CENP-B proteins for *pfl10*, contributes to the stability of *pfl* genes.

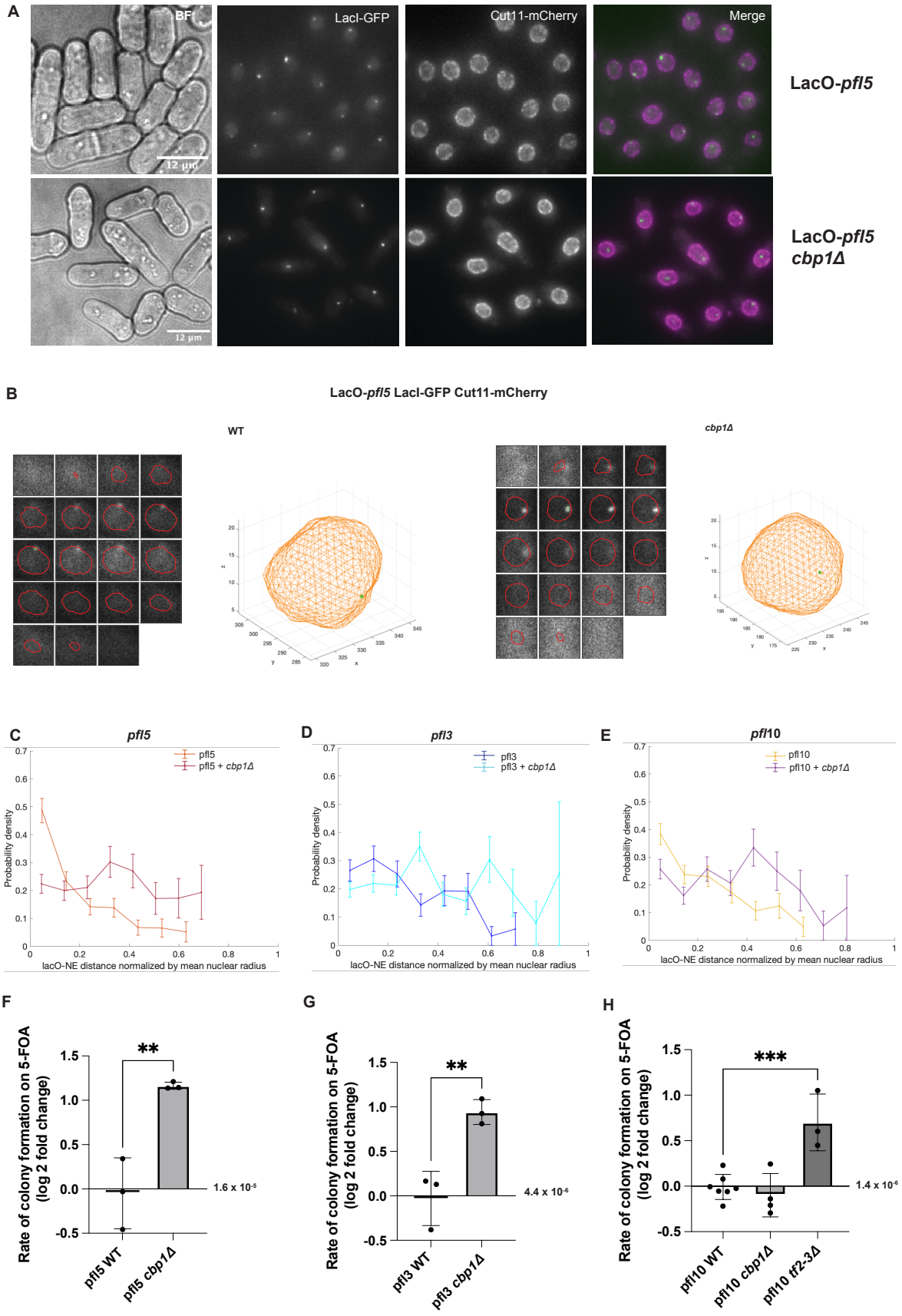
A
BF
LacI-GFP
Cut11-mCherry
Merge
12 µm
LacO-pfl5
LacO-pfl5 cbp1Δ
B
LacO-pfl5 LacI-GFP Cut11-mCherry
WT
cbp1Δ
C
pfl5
pfl5
pfl5 + cbp1Δ
Probability density
lacO-NE distance normalized by mean nuclear radius
D
pfl3
pfl3
pfl3 + cbp1Δ
E
pfl10
pfl10
pfl10 + cbp1Δ
F
Rate of colony formation on 5-FOA (log 2 fold change)
**
1.6 x 10-5
pfl5 WT
pfl5 cbp1Δ
G
**
4.4 x 10-6
pfl3 WT
pfl3 cbp1Δ
H
***
1.4 x 10-6
pfl10 WT
pfl10 cbp1Δ
pfl10 tf2-3Δ

Figure 4. A subset of *pfl* genes are tethered to the nuclear periphery via the CENP B-like protein, Cbp1. A) Using the lacO/lacI-GFP system, we observe that genetically knocking out *cbp1* releases *pfl5* from the nuclear periphery. B) 3D nuclear reconstruction showed that loss of *cbp1* releases the *pfl5* loci from the nuclear periphery across populations of cells. C-E) Probability density functions of the distance from the lacO to the nuclear envelope for *pfl5, pfl3* and *pfl10* with and without Cbp1. Data for WT cells replotted from Fig. 1. F-G) Loss of *cbp1* causes an increase in the rate of recombination at the *pfl5* and *pfl3* loci. A pairwise t-test indicates p=0.0075 for *pfl5* and p=0.0064 for *pfl3.* H) Loss of *cbp1* does not impact the rate of recombination at *pfl*10. However, deletion of *Tf2-3* nearby the *pfl*10 locus leads to an increase in recombination. A one-way ANOVA with Dunnett's multiple comparison test indicates p=0.0007. Data points are the natural log of the fold change in rate.

Cbp1 and the LINC complex cooperate to enforce genetic stability of the *pfl* genes

We previously reported that the nuclear envelope-spanning LINC complex that couples DSBs associated with the nuclear periphery to cytoplasmic microtubule dynamics influences HDR in fission yeast, particularly through the KASH domain protein Kms1 (Swartz, 2014). However, this was in the context of an inducible, irreparable DSB that moved to the nuclear periphery only upon damage induction (Swartz, 2014). We therefore interrogated if loss of *kms1* impacted the stability of *ura4* embedded in the direct repeats of the constitutively peripheral *pfl5* gene and how any observed effect intersected with the influence of *cbp1*. We found that loss of Kms1 increases the rate of colony formation on 5-FOA from 1.53 x 10^{-5} for WT to 2.39 x 10^{-5} for *kms1Δ* cells (Fig. 5A and Table 1). While this increase did not reach statistical significance using an ANOVA test with a Tukey correction for multiple comparisons when comparing all conditions (p=0.15), we obtain a value of p=0.02 using a pairwise t-test of these two conditions alone. To ask whether Kms1 acts in the same pathway as Cbp1, we compared the effect of the single and combined *kms1Δ* and *cbp1Δ* alleles. Similar to the results in Fig. 4F, loss of Cbp1 alone leads to an increase of more than 2-fold in the rate of acquiring 5-FOA resistance (the rate for *cbp1Δ* was 5.06 x 10^{-5}; Fig. 5A and Table 1). There seems to be no additive effect between the two alleles, as *kms1Δcbp1Δ* cells show a rate of 4.73 x 10^{-5}), suggesting that these two factors likely function in the same pathway. Thus, loss of *kms1* appears not to influence this intragenic repair outcome when *pfl5* is released from the nuclear periphery in *cbp1Δ* cells.

In addition to its role in capturing persistent DSBs at the nuclear periphery during the mitotic cell cycle, the LINC complex is also involved in promoting high fidelity homologous chromosome pairing during meiosis across model systems (Conrad et al., 2008; Horn et al., 2013; Lee et al., 2015; Sato et al., 2009; Varas et al., 2015). One model for this function of the LINC complex is that cytoskeletal forces exerted on the chromosomes during meiotic prophase enforce a kinetic proofreading-type mechanism that supports homology testing, possibly by dissolution of non-homologous chromosome pairs (Sato et al., 2009). We therefore considered the possibility that the LINC complex could enforce the use of the homologous repair template (the sister chromatid) during DNA repair by homologous recombination. To test this hypothesis, we created an assay to measure illegitimate recombination between two "homeologous" (similar, but not identical) loci (Fig. 5B). We inserted overlapping halves of the Kanamycin-resistance gene (*kanR*) into two homeologous loci from the same *pfl* gene subfamily (Supplemental Fig. 4) that reside on separate chromosomes, *pfl10* (chromosome I) and *pfl4* (chromosome III); the 5' and 3' regions of *kanR* contained a ~220bp overlap; the *ura4* marker was also inserted to select for the targeted integration. It is important to note that the two copies of *ura4* are in opposite orientations, ensuring that recombination must be driven by the overlap in homology within *kanR* without contributions of the *ura4* sequence. In this assay, use of the homeologous template

during HR allows for the reconstitution of a functional Kan-resistance marker. In WT cells we find that the rate of acquiring Kan-resistance is relatively rare, with a rate of ~2.1 x 10^{-8} (Fig. 5C and Table 1). We found that loss of either *kms1* or *cbp1* causes a significant increase in reconstituting a functional *kanR* cassette, although we observe higher variation in the *cbp1Δ* genetic background (Rate of 6.24 x 10^{-8} for *kms1Δ*, and 6.03 x 10^{-8} for *cbp1Δ*)(Fig. 5C and Table 1). This observation is consistent with tethering to the nuclear envelope (via Cbp1) and/or association with the LINC complex contributing to stringency in selecting the ideal template during repair by homologous recombination.

Last, to provide more insight into the DNA repair mechanism(s) at play, we further investigated the products of DNA repair leading to acquired Kan-resistance. Using PCR primers on either side of *pfl10* or *pfl4* (primers PFL10For, PFL10Rev, PFL4For, PFL4Rev), and both sides of the *kanR* (primers KanUpRev and TEFTermFor), we determined losses and/or gains of genetic material (Fig. 5D). The *kanR* cassette fragments were retained at the starting loci ("product #1" and "product #4") in all conditions tested, arguing against a crossover product. In five representative Kan+ WT isolates we detected no change in the structure at *pfl10* whereas there was a gain of the reconstituted *kanR* cassette at *pfl4*, which is indicated by the gain of a PCR product ("product #3") between the 5' region of the *kanR* and the flanking *pfl4* (unique) coding sequence (Fig. 5D). The simplest explanation for this result is that a spontaneous DSB at *pfl4* led to synthesis-dependent strand-annealing (SDSA) repair event using *pfl10* as a template, resulting in gene conversion. Kan+ isolates acquired in the absence of Cbp1 similarly led to the gain of the *kanR* cassette at *pfl4*. Of note, in one of five examples we tested we also observed a product of the 3' region of the *kanR* at *pfl10* ("product #2"), suggesting that new DNA synthesis occurred at both *pfl4* and *pfl10* leading to reconstitution of an intact *kanR* cassette at both loci. Surprisingly, in five representative *kms1Δ* Kan+ isolates we detected no change at *pfl4* and instead a gain of the 3' region of *kanR* at *pfl10*, suggestive of repair of a DSB at *pfl10* by SDSA using *pfl4* as a template. These observations suggest that although all genotypes reconstitute *kanR* primarily through SDSA, either the spontaneous DSBs driving the repair event and/or their preferred templates are different.

1

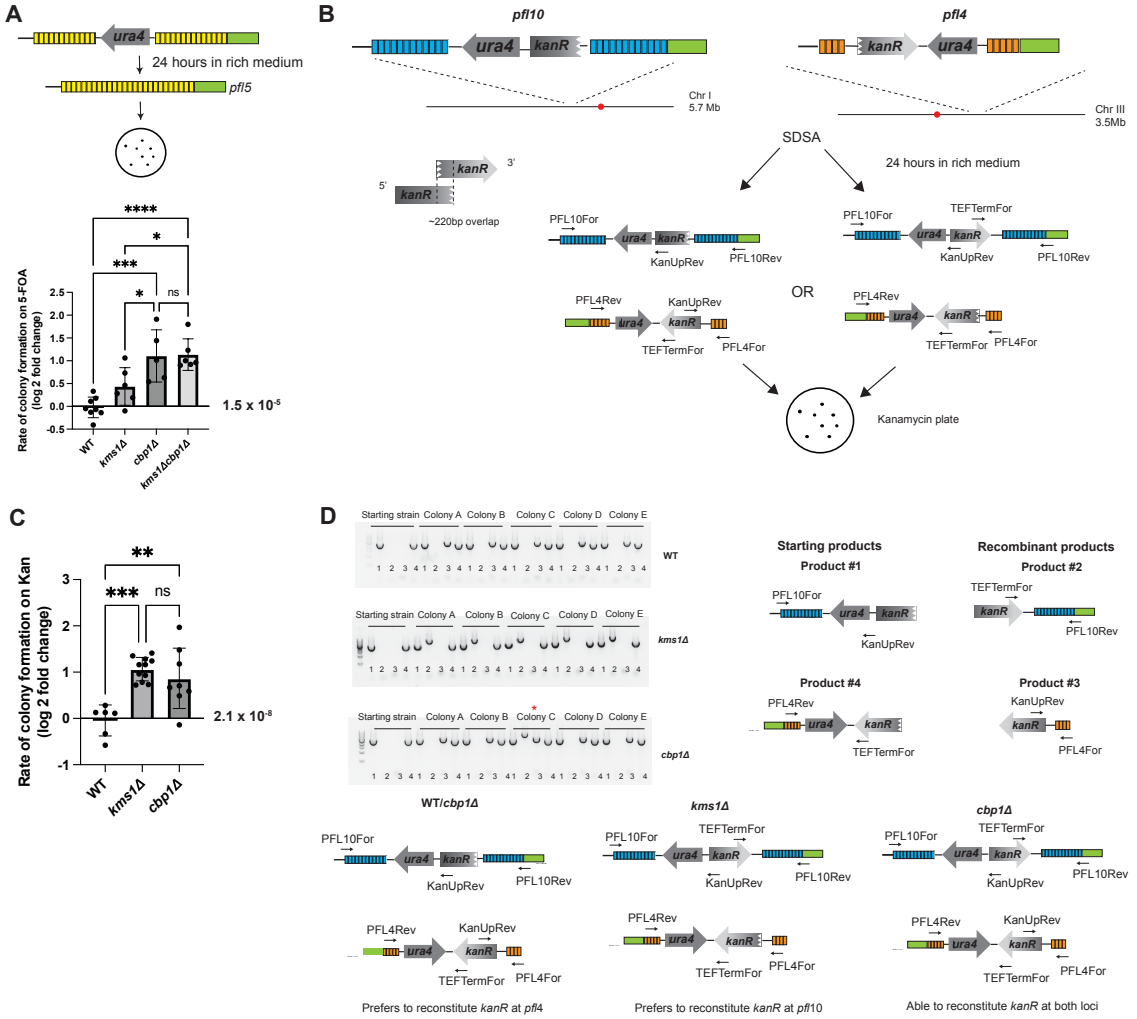

Figure 5. Cbp1 and the LINC complex cooperate to enforce genetic stability of the *pfl* genes. A) Loss of *kms1* increases the rate of colony formation on 5-FOA in the intragenic recombination assay at *pfl5*, although to a lesser extent than loss of *cbp1* (p=0.0002 by one-way ANOVA with a Tukey correction for multiple comparisons). The lack of an additive effect suggests that *kms1* and *cbp1* function in the same pathway to enforce the stability of *pfl5*. Data points are the natural log of the fold change in rate. B) An assay to measure recombination between two homeologous regions. We inserted overlapping halves of *kanR* into homeologous loci *pfl*10 and *pfl*4. Releasing the cells into rich medium allows them to recombine and reconstitute *kanR* at either locus. We measured the rate of recombination between these two regions by measuring the rate of acquiring Kan-resistance. Potential SDSA products are drawn out, along with PCR primers to amplify across the loci to determine the mechanism of acquiring Kan resistance. C) Loss of Cbp1 or Kms1 increases recombination between homeologous loci. The rate of colony growth on Kan plates increases in *cbp1Δ* or *kms1Δ* cells, suggesting that both genes enforce stringency in choosing the correct template during repair by homologous recombination. (p<0.0001 for *kms1Δ* and p=0.0016 for *cbp1Δ* by one-way ANOVA with Dunnett's correction for multiple comparisons.) Data points are the natural log of the fold change in rate. D) PCR products between the *kanR* coding sequence and locus specific primers provided insight into how the cells reconstituted *kanR*. In the starting strain, the 5' side of *kanR* is present at *pfl*10, while the 3' side of *kanR* is present at *pfl*4 ("starting products" #1 and #4). Across all conditions, we observed no loss of starting products, but a gain of recombinant products, suggesting the cells repaired by a non-crossover mechanism, such as SDSA. WT and *cbp1Δ* cells prefer to gain the 5' side of *kanR* at *pfl*4 ("recombinant product" #3), suggesting *kanR* was reconstituted at *pfl*4. However, *kms1Δ* colonies gained the 3' side of *kanR* at *pfl*10 ("recombinant product" #2), suggesting *kanR* was reconstituted at *pfl*10. *cbp1Δ* colonies are also capable of reconstituting *kanR* at both loci (Colony C, see asterisk).

Kms1 antagonizes mutagenic repair

Previous work from our group revealed that Kms1 acts as a suppressor of the growth defect observed in HR-deficient *rad51Δ* cells both on rich medium and in the presence of exogenous DNA damage (Swartz, 2014). However, the mechanism underlying this observation has remained enigmatic. We first sought to test if the improved growth reflects an amelioration of DNA damage load. To this end, we monitored spontaneous DNA repair foci by visualizing Rad52-GFP (Figs. 6A-B). We observed that ~50% of *rad51Δ* cells had at least one Rad52-GFP focus at steady state (Figs. 6A-B). While loss of Kms1 had little effect in its own, consistent with our prior report (Swartz, 2014), its deletion in the context of the *rad51Δ* background led to a marked decrease in spontaneous Rad52-GFP foci to ~25-30% of cells. Interestingly, most WT or *kms1Δ* cells that contained a Rad52 focus were likely in S phase of the cell cycle (indicated by cell length and morphology), while in *rad51Δ* or *kms1Δ rad51Δ* cells Rad52-GFP foci were prevalent in the G2 phase when cells are quite long, indicating that the damage is persistent (Fig. 6B, transmitted light images). Taken together, these results support the idea that loss of Kms1 allows HR-deficient cells to survive in part by ameliorating spontaneous DNA damage, possibly by upregulating another "salvage" DNA repair pathway, as we previously speculated (Swartz, 2014). A pathway able to promote cell survival in the absence of Rad51 in mitotically growing *S. pombe* would be expected to be capable of acting downstream of DSB resection, as essentially all DSBs are committed to HR in this model (Langerak et al., 2011; Leland et al., 2018).

To further investigate this hypothesis, we sought to develop an assay to measure the rate of error-prone DNA repair by creating a pair of inducible DSBs that create incompatible ends, an approach previously used to reveal DNA repair by microhomology-mediated end-joining (MMEJ, also known as alternative end-joining) in budding yeast (Ma et al., 2003b)(Fig. 6C). Specifically, we inserted a *ura4* cassette flanked on both sides by an HO endonuclease cut site into the *mmf1* locus of *S. pombe*, a genomic site that we have previously characterized (Leland et al., 2018). The two HO cut sites are in opposite orientations relative to each other, giving rise to DSB ends that are expected to disfavor repair by cNHEJ. As the assay is built in a haploid strain lacking a template for HR, this arrangement essentially forces the cell to use an alternative mechanism to repair the induced DSB (or to die). We therefore expect that measuring the rate by which viable progeny that have lost functional *ura4* are recovered allows us to calculate the frequency of alternative repair pathway usage. We first explored the sensitivity of the assay to disrupting cNHEJ. Relative to the rate of colony formation on 5-FOA for WT cells of $1x10^{-6}$, a *lig4Δ* genetic background led to a ~50% decrease (Fig. 6D). This raises the possibility that this ligase associated with cNHEJ contributes to a subset of repaired products that have lost *ura4*. However, we note that loss of the cNHEJ factor Pku70 has no effect, consistent with the expectation that the protection of DSB ends, irrelevant in this engineered system, does not play a role.

Consistent with the hypothesis that Kms1 antagonizes an alternative repair mechanism, we observed a three-fold increase in the rate of 5-FOA-resistant colonies in the *kms1Δ* background (Fig. 6D). Taken together, these observations support the idea that the LINC complex restrains cells from using an alternative repair pathway that drives the loss of *ura4* as postulated in our prior work (Swartz, 2014).

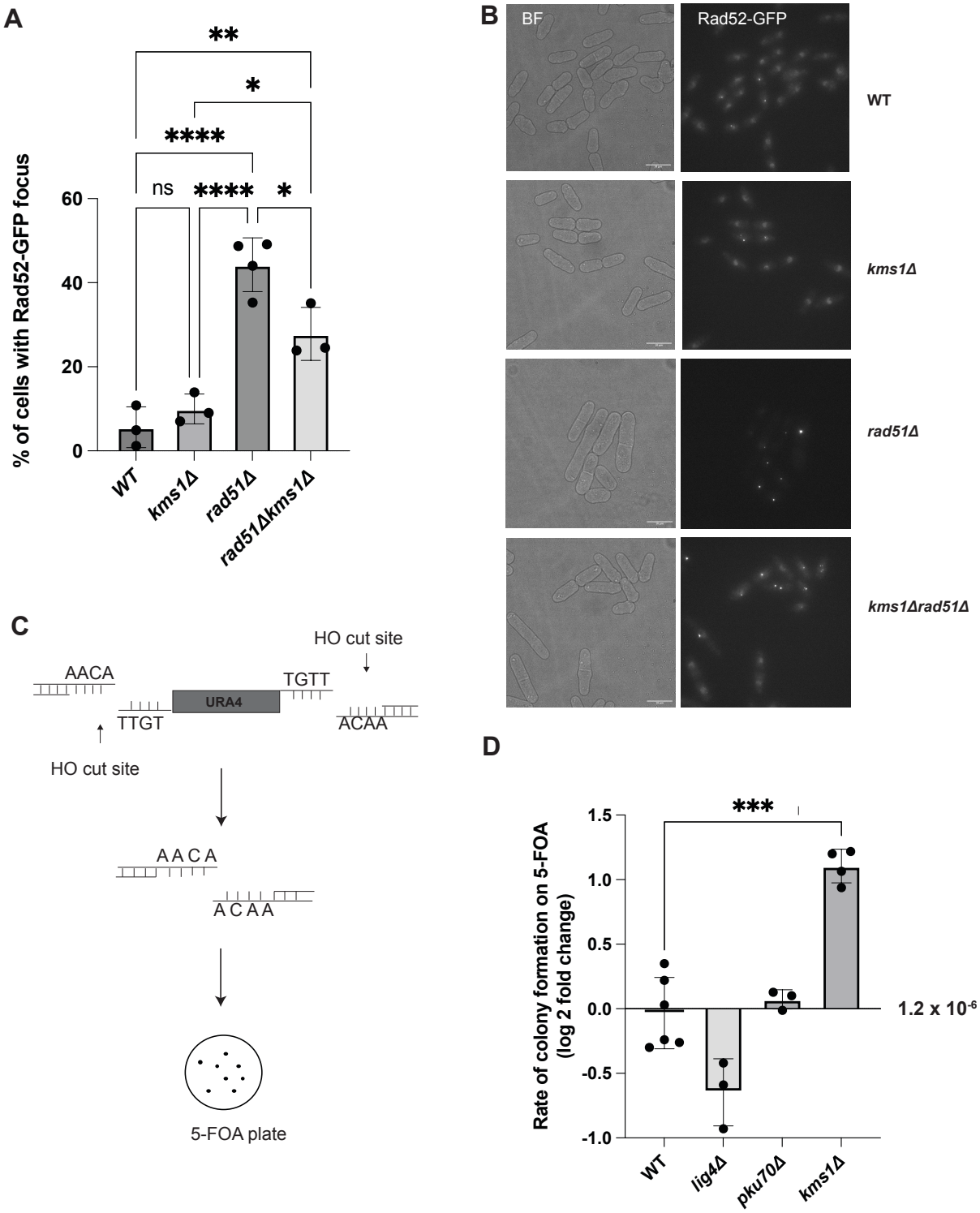
A
**
*
****
ns
****
*
% of cells with Rad52-GFP focus
60
40
20
0
WT
kms1Δ
rad51Δ
rad51Δkms1Δ
B
BF
Rad52-GFP
WT
kms1Δ
rad51Δ
kms1Δrad51Δ
C
HO cut site
AACA
TGTT
URA4
TTGT
ACAA
HO cut site
AACA
ACAA
5-FOA plate
D
***
Rate of colony formation on 5-FOA
(log 2 fold change)
1.5
1.0
0.5
0.0
-0.5
-1.0
1.2 x 10-6
WT
lig4Δ
pku70Δ
kms1Δ

Figure 6. Disrupting *kms1* upregulates likely mutagenic DSB repair A) Analysis of Rad52-GFP foci showed that *kms1Δ* alone has no effect on spontaneous DNA damage, while ~50% *rad51Δ* cells have a Rad52-GFP focus. When *kms1* is also lost from a *rad51Δ* background, the number of foci decreases to ~25-30% (p=0.0158 by one way ANOVA with Tukey correction for multiple comparisons). B) Representative micrographs of Rad52-GFP foci in WT, *kms1Δ*, *rad51Δ*, and *kms1Δrad51Δ* cells. C) An assay to measure the rate of "salvage" repair pathway usage. We created a *ura4* cassette flanked on both sides by an HO-endonuclease cut site. The two cut sites are in opposite orientations, disfavoring cNHEJ. Plating the cells to 5-FOA allowed us to select for cells that have undergone repair and no longer contain a functional *ura4* gene. D) Loss of the cNHEJ ligase Lig4 causes a trend of a decrease in the rate of loss of *ura4*, suggesting Lig4 is involved in this pathway. Although this finding approached statistical significance on an ANOVA with a Dunnett correction for multiple comparisons (p=0.053), a pairwise t-test revealed a p value of p=0.0151. Loss of *pku70* causes no effect, indicating that protection of DSB ends is dispensable in this context. However, loss of *kms1* leads to an increase in the rate of loss of *ura4* (p<0.0001 by one-way ANOVA with Dunnett correction for multiple comparisons), indicating that Kms1 restrains the use of this alternative pathway. Data points are the natural log of the fold change in rate.). * indicates p < .05; ** indicates p < .01; *** indicates p < .001; **** indicates p<.0001

Kms1 restrains the use of an alternative, microhomology-driven repair pathway

One pathway that is important for the survival of HR-deficient cells across model systems is MMEJ (Decottignies, 2007; Lee & Lee, 2007; Sfeir et al., 2024; Truong et al., 2013). Although the fission yeast genome, like budding yeast, does not encode a polymerase with the same structure as the mammalian Pol-θ/PolQ, the use of microhomology upstream of an end joining reaction was first documented in budding yeast (Ma et al., 2003a). We therefore took a sequencing approach to shed light on the type of repair products produced in this alternative repair assay in WT cells and cells lacking *kms1* or *lig4*. To that end, we grew ten individual 5-FOA-resistant isolates from all three genotypes and used colony PCR to amplify across the predicted junction of the two HO cut sites (Fig. 7A). To control for technical failure of the colony PCR including of large products, primers producing a second, 3.5kb control product were included. When using primers annealing ~250 bps outside both sides of the HO cut site-flanked *ura4* insertion (primer pair Mmf1L1+Mmf1L6) we found that WT cells mainly produce a small PCR product of the expected size resulting from loss of the entire sequence between the two HO cut sites (~500bp), although in two of the ten cases (Fig. 7B, red asterisks) we observed a slightly larger product (further discussed below). The 3.5 kb control product is not visible, as the smaller products dominate in the PCR reaction. Interestingly, although the *kms1Δ* background led to six of ten representative products of a similar size to those observed in WT cells, we also observed larger products in some *kms1Δ* isolates, suggesting that *kms1Δ* cells can produce a different type of repair product than WT cells. Similarly, *lig4Δ* cells failed to produce the products that dominate in WT cells, in line with a decrease in overall rate (Fig. 6D), instead revealing a surprising preference for exclusively a large repair product (Fig. 7B). These results raise the possibility that cells lacking *kms1* or *lig4* can access a similar pathway that is disfavored in WT cells.

To further confirm these observations on a greater number of isolates, we prepared a pool of genomic DNA from entire 5-FOA plates of colonies (ranging in number from 30 to 100). With the caveat that smaller products will dominate in the PCR amplification of this pool, we generally confirmed our finding that WT isolates produce expected products in the range of ~500 bps, while *kms1Δ* isolates produce a mixture of WT-like products and products of both larger and smaller sizes (Fig. 7C), suggesting greater flexibility in the types of repair events that lead to viable progeny that no longer express functional *ura4*. To provide greater insight into how loss of *kms1* affects the repair products (likely contributing to the increase in the rate of forming 5-

FOA-resistance colonies, Fig. 6D), we sequenced across the DSB junction in individual isolates that grew on 5-FOA and cloned and sequenced PCR products produced from the pooled genomic DNA. Sequencing of >20 individual isolates revealed that the dominant product in the WT strain (nearly half of all colonies) lost the 4bp overhang left by the HO site 5' to *ura4*, followed by an untemplated insertion of a single T base (Fig. 7D), a hallmark typically ascribed to cNHEJ (Decottignies, 2007; Manolis et al., 2001). Notably, a similar chromosomal DSB repair assay in fission yeast revealed a single A base insertion in the dominant repair product in WT cells, which was found to be dependent on Lig4 (Li et al., 2012). The remainder of WT colonies exhibited diverse, small losses of sequence ranging from 3bp to 10bp (Fig. 7D). Given that most products in WT cells do not seem to involve microhomology (Supplemental Fig. 5A), the rate of producing 5-FOA-resistant colonies is lower in *lig4Δ* cells (Fig. 6D), and these repair outcomes were not observed in cells lacking *lig4* (Fig. 7B), the predominant mechanism at play in WT cells appears to be consistent with a cNHEJ-like mechanism (Fig. 7D).

Focusing first on *kms1Δ* isolates that produce a similarly sized product to WT, we observed small losses of sequence at the junction of the two HO sites (Fig. 7D), but notably no untemplated insertions that resemble the dominant, cNHEJ-like product in WT cells. Indeed, we only observed rare products in common between WT and *kms1Δ* isolates (Fig. 7D, black lines), further suggesting that cells lacking Kms1 might engage a distinct mechanism that is less like cNHEJ. To further characterize the larger (>2kb) repair product in *kms1Δ* cells, we cloned and sequenced the dominant species. Interestingly, these products appeared to result from the cleavage of only one of the two HO recognition sites. While the HO site 3' to *ura4* remains intact, the site 5' to *ura4* is destroyed. The junction appeared to result from rejoining to microhomology within the gene body of *ura4*, leading to loss of hundreds of base pairs of sequence (Supplemental Fig. 5B). These cells therefore retain a portion of the *ura4* sequence but become resistant to 5-FOA due to the non-functional protein product. The slightly larger WT products (Fig. 7B, asterisks) are also the result of cleavage of only one HO cut site, but notably the only "single cutter" product in WT results in near complete loss of the *ura4* sequence, as opposed to *kms1Δ* cells where a greater span of the *ura4* gene is maintained. This result suggests that cells lacking *kms1* are more able to use microhomologies within *ura4* to drive repair when a single HO cut site is cut, consistent with the elevated overall rate of generating *ura4*-deficient colonies (Fig. 6D). Interestingly, sequencing across the DSB junction in *lig4Δ* cells revealed that both HO cut sites were intact in all samples, suggesting that either "spontaneous" DSBs within the *ura4* were repaired in an error-prone fashion (while those cut at the HO sites could not be repaired and were therefore lost due to lethality) or that DSBs at the HO cut sites were repaired efficiently by another ligase. Interestingly, however, products from *lig4Δ* cells also showed a loss of sequence at *ura4* similar to the *kms1Δ* "single cutter" samples. These DSBs were repaired by a 4bp microhomology within the *ura4* gene body (Supplemental Fig. 5C), causing the loss of hundreds of base pairs of sequence internal to *ura4* and a non-functional protein product. We disfavor the interpretation that these products are truly "spontaneous", however, because we failed to recover any colonies on 5-FOA in the absence of DSB induction. Similar products were also detected in *kms1Δ* cells in which repair proceeded by a 2bp microhomology (Supplemental Fig. 5B), indicating that this type of repair is also possible when *lig4* is present, although end-joining using the HO site still dominates in this context. Importantly, we never observed the retention of both HO cut sites in WT cells, suggesting that loss of *kms1*. Taken together, these

observations suggest that Kms1 (and therefore a functional LINC complex) normally antagonizes repair by Lig4-independent mutagenic end joining in fission yeast (Fig. 7E).

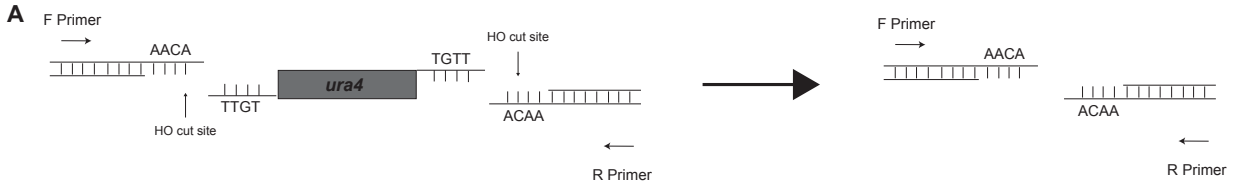

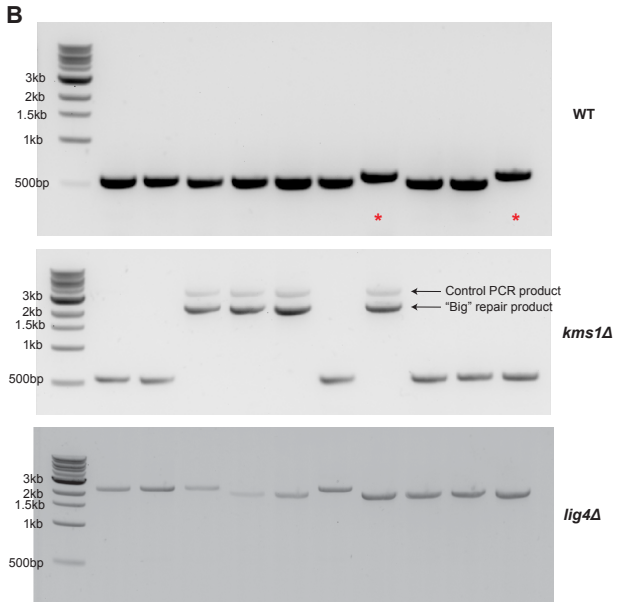

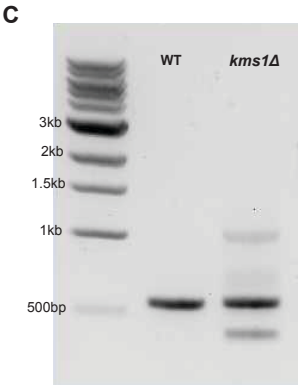

D

WT

Sequence	Product	Prevalence
5′-CCGCAACATGTTGCGG-3′	(Expected product from perfect end-rejoining)	
5′-CCGC-----TTGTTGCGG-3′	-4bp, +1bp	43.4% (10/23)
5′-CCGCAACA------GCGG-3′	-4bp	17.4% (4/23)
5′-CCGCAACA----TGCGG-3′	-3bp	13% (3/23)
5′-CCGC----------GG-3′	-10bp	8.7% (2/23)
5′-CCGCA-------GTTGCGG-3′	-4bp	4.34% (1/23)
5′-CCG----------TTGCGG-3′	-6bp	4.34% (1/23)
5′-CCGCAA---------TGCGG-3′	-5bp	4.34% (1/23)
5′-CCGCA-----TGTTGCGG-3′	-3bp	4.34% (1/23)

kms1Δ

Sequence	Product	Prevalence
5′-CCGCAACATGTTGCGG-3′	(Expected product from perfect end-rejoining)	
5′-CCGC--------GTTGCGG-3′	-5bp	9/20 (45%)
5′-CCGC----------CGG-3′	-9bp	4/20 (20%)
5′-CCGCAACA-----TGCGG-3′	-3bp	2/20 (10%)
5′-CCGCA-----TGTTGCGG-3′	-3bp	2/20 (10%)
5′-CCGCAAC----------GG-3′	-7bp	1/20 (5%)
5′-CCGCAA---------TGCGG-3′	-5bp	1/20 (5%)
5′-CCGC--------TGTTGCGG-3′	-4bp	1/20 (5%)

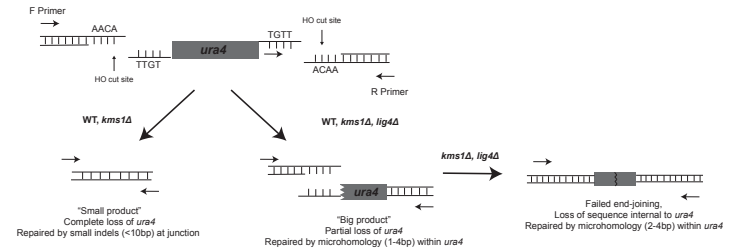

1

Figure 7. Kms1 restrains the use of a "salvage" DNA repair pathway that involves microhomologies. A) Analysis approach for 5-FOA-resistant colonies. After HO nuclease induction and FOA selection, we extracted gDNA from individual FOA+ colonies and PCR amplified across the junction using primers outside of the DSB junction. B) PCR amplifying across the junction of the HO sites in single FOA+ colonies showed genotype-specific repair product preferences. WT cells produce a small product of expected size resulting from loss of the entire sequence between the two cut sites (~500bp), with slightly larger products also observed (red asterisks). In *kms1Δ* cells, however, a subset of cells produce WT-like small products, while another subset produces larger products, which are similar to products observed in the *lig4Δ* background. To control for technical failure of the colony PCR, a 3.5kb "control product" was also generated. C) PCR amplifying across the junction of the HO sites from a pool of genomic DNA from entire plates of colonies confirmed our finding that WT colonies predominantly produce only the expected product size while *kms1Δ* colonies produce a mixture of products. D) In WT cells, the most common product of a salvage DNA repair pathway is the loss of the entire *ura4* gene and the 4bp overhang left by the HO site 5' to *ura4*, and the untemplated insertion of a single T base. WT also exhibits small losses of sequence (ranging from 3-10bp) at the junction of the two HO sites. The *kms1Δ* colonies that produced a similarly sized product to WT were small losses of sequence at the junction of the two HO sites, but no untemplated insertions were observed. Three products were observed in both genetic backgrounds (black bars). E) Sequencing analysis revealed multiple products of DNA repair: 1) "small products", produced only in WT and *kms1Δ* cells, which are the result of cleavage of both HO sites, loss of the entire *ura4* sequence, and rejoining with small deletions/insertions at the DSB junction, as outlined in panel D; and 2) "big products" where the 5' HO site is destroyed but the 3' site is retained, and a portion of the *ura4* sequence is retained. These products are possible by rejoining within a microhomology within the *ura4* gene body. In a *lig4Δ* background, neither end of the DSB is able to simply rejoin, requiring the cell to repair using microhomology within the *ura4* gene leading to loss of a portion of the sequence internal to *ura4*. These products are also possible in *kms1Δ* cells, further supporting the idea that *kms1Δ* cells can produce a variety of products.

In summary, this sequencing analysis revealed that in the absence of a homologous template, WT cells prefer to use a "cNHEJ-like" repair pathway whose dominant product is an untemplated insertion at the DSB junction, in addition to the loss of all sequence between the two DSB sites. WT cells can also occasionally repair using microhomology with *ura4*. In cells lacking Kms1 we observe an increase in the potential microhomologies that can be used for repair (which explains both the increase in rate (Fig. 6D) and the variety of products seen in the *kms1Δ* versus WT cells (Figs. 7B-D). These microhomologies may be Lig4-independent, as *kms1Δ* cells are capable of creating repair products similar to *lig4Δ* cells. Taken together, these results suggest that Kms1 restrains the use of a salvage DNA repair pathway that repairs using Lig4-independent microhomologies. Although mutagenic, access to this pathway likely allows cells to survive conditions in which HR is severely compromised, including those lacking Rad51 (Figs. 5A-B).

Discussion

The high fidelity of homology-directed repair depends on the cell's ability to select the correct homologous template, which can be particularly challenging for DSBs that occur in repetitive regions of the genome. In this work, we leveraged the *S. pombe* flocculin-like gene family as a model to study mechanisms that contribute to genome integrity in repetitive coding genes, as their modular sequences make them prone to instability and intragenic recombination. We identified two factors that influence the fidelity of homology-directed repair outcomes in these gene family: 1) the CENP-B like protein Cbp1, which constrains the *pfl* genes to the nuclear periphery and enforces their stability, and 2) the LINC complex component Kms1, which connects DSBs at the nuclear periphery to dynamics driven by the cytoplasmic microtubule cytoskeleton and disfavors use of homeologous templates or microhomology-mediated repair. Our observations provide evidence that genome organization contributes to the stability of protein repeat-encoding genes, specifically through constitutive association with the nuclear periphery, while Kms1 enforces stringency in homology-directed repair and antagonizes use of microhomologies, potentially for any DSB that associates with the LINC complex.

Stability of the *pfl* genes is tied to *Tf2* transposons, Cbp1, and the nuclear periphery

Previous work across model systems suggests that cells leverage nuclear compartmentalization to enforce faithful repair of difficult to replicate regions of the genome, including those that are repetitive such as the centromeres, telomeres, and rDNA (Lemaître et al., 2014; Torres-Rosell et al., 2007; Tsouroula et al., 2016). Specifically, DSBs in such genomic regions will move out of their "recombination-repressive" zone of the nucleus into subnuclear regions that are favorable to recombination, such as the NPC (Chiolo et al., 2011; Churikov et al., 2016; Horigome et al., 2016; Kalocsay et al., 2009; Kramarz et al., 2020; Nagai et al., 2008; Oza et al., 2009; Ryu et al., 2015; Tsouroula et al., 2016). Our findings extend these studies by supporting the idea that tethering of repetitive protein coding genes to the nuclear periphery likewise protects their stability. We demonstrated that most *pfl* genes analyzed constitutively reside at the nuclear periphery through a mechanism involving the *Tf2* transposons and/or their LTRs and the LTR-binding factor, Cbp1 (Figs. 1, 3, and 4). Employing an assay to measure the stability of the loci encoding members of this gene family, we found that repeat number is correlated with their level of instability (Fig. 2), consistent with prior studies (Verstrepen & Klis, 2006; Zhao et al., 2017). We provide evidence that loss of Cbp1 leads to untethering of *pfl5* from the nuclear periphery that we tie to an increase intragenic recombination (Fig. 4); loss of Cbp1 likewise enhances the instability of *pfl3* (Fig. 4). While we observe a more muted effect of abrogating Cbp1 on the position and stability of *pfl10*, we observe that deletion of the nearby *Tf2-3* transposon also enhances repeat instability (Fig. 4). Taken together, these observations suggest that the stability of members of the *pfl* gene family could be coupled, by virtue of their proximity to transposable elements or their remnants (LTRs), to the biology of transposons. As *Tf2* elements are known to cluster in the nucleus in a mechanism that suppresses their mobilization (Cam et al., 2008; Lorenz et al., 2012; Murton et al., 2016), and there is evidence that propagation of the *Tf2* transposons in *S. pombe* rely on HR (Hoff et al., 1998), one attractive hypothesis is that *S. pombe* leverages adaptive mechanisms to restrain transposon activity to stabilize host repetitive coding genes. Indeed, a recent study provides evidence that transposons in *S. pombe* contribute to the fitness of the "host" (Cranz-Mileva et al., 2024). In addition to reducing intragenic recombination of the *pfl* genes, we also observe that Cbp1 restrains intergenic recombination

between the related *pfl4* and *pfl10* (Figs. 5C-D). In addition to the effects observed in the intragenic recombination reporter assays, Cbp1 might also further restrain the likelihood that two *pfl* genes can encounter one another after a spontaneous DSB arises by virtue of their tethering to the nuclear periphery as the probability of a physical encounter between the DSB and template is thought to play a strong contribution to template choice during HR (Wang et al., 2017).

Kms1 enforces the fidelity of homology-directed repair

Most *pfl* genes reside at the nuclear periphery constitutively (Fig. 1), but we also previously demonstrated that slow to repair DSBs are also targeted to the inner nuclear membrane SUN protein, Sad1, in fission yeast; a subset of these Sad1-engaged DSBs also assembled full LINC complexes that include the KASH protein/Nesprin orthologue, Kms1 (Swartz, 2014). The stability of *pfl5* appears to be dominated by the effect of Cbp1, as although we observe a trend towards elevated intragenic recombination at *pfl5* in cells lacking Kms1, it is more muted than the effect of Cbp1. The combination of these two alleles recapitulates the effect of loss of Cbp1 alone (Fig. 5A). However, we observe that loss of Kms1 not only enhances the likelihood of an intergenic repair event between *pfl4* and *pfl10* (Figs. 5B-5C), but that it also alters the recombination products (Fig. 5D). It is not yet clear why cells lacking Kms1 prefer to reconstitute *kanR* at *pfl10* rather than *pfl4*, which dominates in WT cells (Fig. 5D). One possibility is that this result reflects a more prominent role for Kms1 in antagonizing this homeologous strand invasion event occurring between a spontaneous DSB at *pfl10* and the donor sequence at *pfl4*. However, it is also plausible that the loss of Kms1 influences the relative likelihood that a spontaneous DSB arises at these two loci.

In terms of the mechanism by which Kms1 antagonizes this non-allelic repair event, there are parallels with prior work suggesting that the LINC complex enforces stringency in homologous chromosome pairing during meiosis, originally documented in *C. elegans* (Sato et al., 2009). Across models, there is a conserved role for the cytoplasmic cytoskeleton in exerting forces on the chromosomes during meiotic prophase via LINC complexes, typically involving microtubules (although actin serves this function in budding yeast (Chiolo et al., 2025)). In such a model, LINC complexes could promote dissolution of stand invasion structures without sufficient homology in a kinetic proofreading-type mechanism thereby enforcing stringency in template choice during any type of homology-directed repair.

The LINC complex restrains mutagenic MMEJ

Consistent with a physical model in which Kms1 promotes dissolution of repair intermediates lacking sufficient homology, at an irreparable DSB Kms1 appears to antagonize end joining, as we observe up-regulation of repair events leveraging microhomologies in *kms1Δ* cells (Fig. 6D; Fig. 7C-E). This observation provides an explanation for our previous finding that loss of Kms1 can suppress the growth defect of *rad51Δ* cells (Swartz, 2014). In line with this, we found that loss of Kms1 indeed decreases the frequency of spontaneous Rad52 foci exhibited in recombination-defective, *rad51Δ* cells (Figs. 6A-B). These results support the idea that a Rad51-independent repair mechanism is up-regulated upon loss of fully-assembled LINC complexes. Using a system employing two inverted site-specific DSBs to enforce incompatible ends (Fig. 5C), we observe that WT cells repaired primarily with an untemplated insertion of a single T base at the junction of the two DSB ends (Fig. 7D), a hallmark of cNHEJ. This result is further reinforced by the results of another chromosomal DNA repair assay in fission yeast, where the

dominant repair product was the insertion of a single A base (Li et al., 2012). This study also reported that this product was lost in mutants of *lig4*, the primary ligase in cNHEJ, reinforcing the idea that this is a cNHEJ product. This is consistent with our observation of a decrease in the frequency of repair in this assay in *lig4Δ* cells (Fig. 6D). Moreover, our inability to detect the dominant WT cell product in *lig4Δ* cells further supports this interpretation. Instead, we observe that loss of *lig4* leads to an alternative repair outcome that drives an internal deletion in *ura4* with junctions containing a 4 bp microhomology (Supplemental Fig. 5).

Along with greater proficiency in repairing these incompatible DSB ends, *kms1Δ* cells also disfavor the cNHEJ-like single base pair insertion (Fig. 7D). Instead, we observe a greater variety of repair products of varying sizes that result from microhomology within the *ura4* gene body (Figs. 7B-7C and Supplemental Figs. 5B-C). Taken together, these results support the idea that the LINC complex restrains the use of repair by the mutagenic, *lig4*-independent, MMEJ pathway, which cells will use when recombination with a homologous template is not possible.

We anticipate that this "incompatible DSB ends" assay will be broadly useful as, in combination with genetics, it provides a facile system in which to study the role of various genes on MMEJ in fission yeast. It will be interesting to learn how early HR factors (such as Mre11 and Ctp1) impact repair frequency and outcome, as previous work has identified roles for these factors in a related assay in budding yeast (Lee & Lee, 2007). It would also be interesting to study other proteins known to be involved in MMEJ in other systems, such as flap nucleases (FEN1 in humans, Rad27 in budding yeast, and Rad2 in fission yeast), particularly because mutations in Rad27 have been shown to increase instability of repetitive regions of the genome of budding yeast (Liu et al., 2004). However, some differences are likely to be observed as well. For example, a prior study evaluated MMEJ using an extrachromosomal DNA repair assay in fission yeast, finding roles for HR factors including Rad52, Rad51, and Exo1 (Decottignies, 2007). These differences could arise due to differences in the repair of an extrachromosomal DSB compared to one occurring in the chromatin.

Overall, our findings propose two mechanisms that enforce the maintenance of genome integrity in fission yeast, particularly in repetitive regions of the genome. First, we find that tethering repetitive, protein-coding genes to the nuclear envelope via the transposon-binding protein, Cbp1 restrains both intragenic recombination and a non-allelic recombination event between homeologous genes. Kms1, the cytoplasmic aspect of the LINC complex relevant to DSB repair in fission yeast (Swartz, 2014), similarly represses illegitimate recombination events within and between repeat-encoding genes as well as mutagenic MMEJ when recombination is inhibited. These mechanisms contribute to the broad evidence that nuclear compartmentalization helps to ensure faithful DNA repair.

Materials and Methods

Microscopy

For lacO localization, images were acquired on a DeltaVision wide-field microscope (Applied Precision/GE) using a 1.2 NA 100x objective (Olympus), solid-state illumination, and an Evolve 512 EMCCD camera (Photometrics). Cells were mounted on 1.2% agar pads and sealed with VALAP (1:1:1 vaseline:lanolin:paraffin). Imaging parameters were as follows. Transmitted light: 50% transmittance, 0.025s exposure; mCherry: 50% power, 0.1s exposure; GFP: 50% power, 0.01s exposure. 40 Z-sections were acquired at 0.26mm spacing.

For spontaneous Rad52 foci, images were acquired on the same microscope and objective but with a CoolSnap CCD camera. Cells were mounted directly on a glass slide. Imaging parameters were as follows: Transmitted light: 32% transmittance, 0.015s exposure; mCherry: 32% power, 0.1s exposure; GFP: 32% power, 0.1s exposure. 16 Z-sections were acquired at 0.4mm spacing.

3D particle localization and image analysis for 3D nuclear reconstruction

We determined the position of GFP-labeled genomic loci from a set of 2D microscope images collected at multiple equally-spaced focal depths (z-stack). To estimate the 2D positions within the plane of the microscope field of view, we generate a maximum intensity projection over all 2D images (z-slices). We then estimate the 2D positions of each locus to pixel level accuracy by thresholding and keeping only the local maximum intensity within a given radius of 1.5 pixels, which is sufficient to encompass each locus. We then select a region around the estimated locus position from the full z-stack and perform a least-mean-squares fitting of a 3D Gaussian within the selected region to determine the best-fit position of locus. We used a previously developed image analysis pipeline outlined in our previous work(Zhao et al., 2016). The GitHub folder with the code can be found here:
https://github.com/mochrielab/3DMembraneReconstruction. In this pipeline, we first generate an initial spherical mesh for each nucleus with a radius calculated based on the nuclear area of the 2D projection of the z-stack. We then modify the vertices of the mesh to minimize the total energy, which consists of the bending energy of the surface and an energy cost related to how well the shape describes images in the entire z-stack.

Probability density calculation

We calculated the probability densities for Figs. 1 D and E, Figs. 4 C, D, and E, and Supplemental Fig. 3 as follows. First, we scaled the coordinates for each cell by the corresponding nuclear radius. Then, we partitioned each scaled nucleus into concentric shells of width, w, equal to 0.1 of the scaled nuclear radius. Next, we determined the probability, p, that each locus of interest is observed in the shell at scaled radial coordinate, r. Then, the probability density, f, is p divided by the scaled volume of the corresponding shell: $f = p/(4\pi r^2 w)$. The scaled distance from the nuclear envelope, s, is the complement of the scaled radial coordinate, i.e. $\mathrm{s} = 1 - \mathrm{r}$. Figs. 1 D and E, Figs. 4 C, D, and E, and Supplemental Fig. 3 plot $f = p/(4\pi(1-s)^2 w)$ versus s. Since p, r, s, and w are all dimensionless, so is the probability density in this case.

Yeast culture and strain construction

S. pombe cells were grown, maintained, and crossed using standard procedures and media (Moreno et al., 1991). Gene replacements were made by gene replacement with various MX6-based drug resistance genes (Bähler et al., 1998; Hentges et al., 2005). For lacO strains: plasmids

previously designed in our group, pSR10_ura4_5.6kb that contain a series of lacO repeats 5.6kb in length (Leland & King, 2014) were targeted to various *pfl* genes using the primers listed in the table below. For intragenic and intergenic/homeologous recombination strains: megaprimers were amplified from pFA6a-Kan that contained opposite halves of the Kanamycin-resistance gene (with ~220bp of overlap between them), with homology arms to target *ura4* in the plasmid pAW1. These megaprimers were used to amplify *ura4* from plasmid pAW1 using iProof polymerase, creating a cassette that contained both halves of the Kanamycin-resistance gene and *ura4*. This cassette was targeted to various *pfl* genes (*pfl3*, *pfl4*, *pfl5*, *pfl*10, *mam3*, *map4*) of *S. pombe*.
For salvage DNA repair assay strains: pFA6a_HOcs_Ura_HOcs was integrated into the *mmf1* locus of *S. pombe* using the primers Mmf1L1 and Mmf1L6 listed in the table below.

Plasmid construction

For salvage DNA repair assay: we modified a plasmid from a previous study (Leland et al., 2018) which contained a modified MX6-based hygromycin-resistance cassette containing the HO cut site (pFA6a-HOcs-Hyg). Construction of this plasmid consisted of two cloning steps: First, the marker on pFA6a-HOcs-Hyg was switched from the hygromycin-resistance gene to the *S. pombe ura4* gene. To carry out the marker switch, pFA6a-HOcs-Hyg was cut at AscI and PmeI to release the Hyg-resistance gene fragment. An insert with the *S. pombe ura4* gene was created by amplifying *ura4* from a pFA6a-Ura4 with primers containing AscI and PmeI cut sites on either end: Ura4_ins_AscI and Ura4_ins_PmeI. PCR conditions are as follows: 3 minute initial denaturation at 95°C, 35 times cycling at 95 °C for 30 second denaturation, anneal at 55°C for 30 seconds, and extend at 72°C for 2 minutes. Final extension for 3 minutes at 72°C. The insert was ligated into the digested plasmid and transformed into DH5a competent cells. Colonies were miniprepped with the Qiagen Miniprep Kit and sent for sequencing to screen for insertion, giving rise to plasmid pFA6a_HOcs_Ura. The second cloning step was to add another HO cut site into pFA6a_HOcs_Ura on the opposite side of the *ura4* insert in the opposite orientation of the existing HO cut site. For this, pFA6a-HOcs-Ura4 was cut at AscI. An insert for the HO cut site was created by annealing the following complementary pre-phosphorylated oligonucleotides containing AscI cut sites on both ends: HOcs_ins_AscI_F and HO_ins_AscI_R. The new insert was digested with AscI, then ligated to the plasmid and transformed into DH5a competent cells. Colonies were miniprepped with the Qiagen Miniprep Kit and sent for sequencing to screen for the insert. Care was taken to ensure the HO cut sites were in opposite orientations giving rise to pFA6a_HOcs_Ura_HOcs. The cassette was amplified using iProof polymerase-based PCR with the primers Mmf1L1+Mmf1L6 using the following PCR protocol: 3 minute initial denaturation at 98°C, 30 times cycling at 98°C for 30 second denaturation, anneal at 52 °C for 10 seconds, and extend at 72°C for 1 minute and 30 seconds. Final extension for 5 minutes at 72 °C. The cassette was transformed into the *mmf1* locus of *S. pombe* using standard procedures.

Assay for measuring instability at repetitive regions of *pfl* family genes

Single colonies were picked from strains that were maintained on EMM-Ura medium. They were grown in 5mL YE5S medium at 30 °C for 24 hours. They were then plated to 5-FOA (diluted 1:100) and YE5S (diluted 1:10,000,000). After 3 days at 32 °C, the colonies on both plates were counted to calculate the rate of loss of *ura4*. Fold change in rate was calculated by dividing each individual rate by the mean rate in WT. All plots show the natural log of the fold change in rate.

Assay for measuring homeologous recombination

Cells that were maintained on EMM-Ura were grown in 5mL YE5S medium at 30 °C over the day, then diluted 1:10 (to a total culture volume of 50mL) and allowed to grow at 30 °C overnight. They were then plated to YE5S+Kan and YE5S (diluted 1:6,000,000). After 3 days at 32 °C, the colonies on both plates were counted to calculate the rate of acquiring Kan resistance. Fold change in rate was calculated by dividing each individual rate by the mean rate in WT. Plots show the natural log of the fold change in rate. To amplify the products of homeologous recombination, gDNA was extracted from Kan+ colonies using the phenol/chloroform method. 1µg of this gDNA was included in a 2X Long Amp Taq PCR reaction, along with primers to amplify across both loci and the kanamycin-resistance gene. For the starting products, the following primer pairs were used: PFL10For + KanUpRev ("product #1") and PFL4Rev + TEFTermFor ("product #4"). For the recombinant products the following primer pairs were used: PFL10Rev + TEFTermFor ("product #2") and PFL4For+ KanUpRev ("product #3). PCR conditions were as follows: 13 minute initial denaturation at 95°C, 30 times cycling at 95 °C for 30 second denaturation, anneal at 52 °C for 30 seconds, and extend at 65°C for 5 minutes. Final extension for 10 minutes at 65°C.

Assay for measuring salvage DNA repair pathways

Cells that were maintained on EMM-Ura were transformed with pREP81HO (Prudden et al., 2003) using the lithium acetate method and plated onto EMM-Ura-Leu+Thi (-Leu to select for uptake of the pREP81HO plasmid, and +Thi to repress the expression of the HO endonuclease under the control of the nmt41 promoter). A subset of colonies from that plate (~10-30) were grown together in 50mL EMM-Ura-Leu+Thi overnight at 30 °C. The following day, the entire culture was spun down and washed twice with water (to wash out the thiamine). Cultures were then diluted in EMM-Leu to OD 0.05 and allowed to grow at 30 °C over the day. Releasing the cells into thiamine-free medium allowed the expression of the HO nuclease, and thus, the induction of cutting at the HO recognition site. To prevent culture saturation and to allow the cells to continue cycling, cultures were diluted to OD 0.05 at 8 hours, 24 hours, and 32 hours post-thiamine wash. 48 hours post-thiamine wash, the entire culture were plated onto 5-FOA and YE5S (diluted 1:2,000,000). After 3 days at 32 °C, the colonies on both plates were counted to calculate the rate of loss of *ura4*. Fold change in rate was calculated by dividing each individual rate by the mean rate in WT. Plots show the natural log of the fold change in rate.

Sequencing

To sequence across the junction of the HO cut sites, we designed primers approximately 250bp from each HO cut site at the gene *mmf1* (Mmf1L1+Mmf1L6). These primers were used to amplify across the DSB junction for each colony that grew on 5-FOA to screen for the size of the junction via colony PCR with 2X Long Amp Taq. An additional primer set (Aly3F and Aly3R in the primer table) of primers were used as a technical control for the colony PCR. PCR conditions are as follows: 13 minute initial denaturation at 95°C, 30 times cycling at 95 °C for 30 second denaturation, anneal at 52 °C for 30 seconds, and extend at 65°C for 2 minutes. Final extension for 10 minutes at 65°C. For colonies that produced a positive result, genomic DNA was extracted using the phenol/chloroform method and another PCR (Taq-polymerase based) was performed using the same primer pair across the DSB junction to prepare for sequencing. PCR conditions are as follows: 5 minute initial denaturation at 95°C, 35 times cycling at 95 °C for 30 second

denaturation, anneal at 52 °C for 30 seconds, and extend at 72°C for 2 minutes. Final extension for 5 minutes at 72°C. PCR products were purified with the Qiagen PCR Purification Kit and sent for sequencing to the Yale Keck Sequencing Center with the sequencing primer L1Seq. Twenty "small products" were sequenced from WT and *kms1Δ* strains. For "big products", the purified PCR product was TA cloned into a pCR 2.1 vector using the Invitrogen TOPO TA Cloning Kit and transformed into competent DH5a cells. Plasmid DNA was purified with the Qiagen Miniprep Kit. Plasmids were digested with EcoRI to determine the size of the insert. Plasmids were sent for sequencing to the Yale Keck Sequencing Center.

Acknowledgements

We would like to thank all members of the LusKing Lab for discussion and feedback, particularly Dr. Connor McBrine. We thank Elisa Rodriguez for technical expertise and support. We also thank the Yeast Genome Resource Center at Osaka University and the many investigators who have deposited strains at this resource. We thank the Keck DNA Sequencing Facility at Yale for their assistance. This work was supported by DP2OD008429 and R35GM153474 (to MCK), EFMA-1830904 (to MCK and SGJM) and T32GM007499 and F31GM143917 (to AL).

Intragenic recombination	
Genotype	**Rate of recombination**
pfl3:3'kan-ura4+	$4.39 \times 10^{-6} \pm 9.88 \times 10^{-7}$
pfl10:ura4+-5'kan	$1.41 \times 10^{-5} \pm 3.55 \times 10^{-6}$
pfl5:ura4+-5'kan	$1.53 \times 10^{-5} \pm 5.35 \times 10^{-6}$
map4 200-3:ura4+-5'kan	$1.59 \times 10^{-6} \pm 8.38 \times 10^{-7}$
mam3 201-1:3'kan-ura4+	$5.25 \times 10^{-6} \pm 4.22 \times 10^{-6}$
pfl5:3'kan-ura4+ lig4Δ::kanMX6	$7.83 \times 10^{-6} \pm 8.34 \times 10^{-7}$
pfl5:ura4+-5'kan exo1Δ::kanMX6	$1.14 \times 10^{-5} \pm 1.56 \times 10^{-6}$
pfl5:ura4+-5'kan rad52Δ::kanMX6	$6.70 \times 10^{-5} \pm 4.88 \times 10^{-5}$
pfl5:ura4+-5'kan rad51Δ::hygMX6	$8.17 \times 10^{-4} \pm 1.19 \times 10^{-4}$
pfl5:ura4+-5'kan rad55Δ::hygMX6	$1.22 \times 10^{-4} \pm 1.68 \times 10^{-5}$
pfl5:ura4+-5'kan swi10Δ::kanMX6	$4.39 \times 10^{-5} \pm 2.2 \times 10^{-5}$
pfl5:3'kan-ura4+ cbp1Δ::kanMX6	$5.06 \times 10^{-5} \pm 1.68 \times 10^{-6}$
pfl3:3'kan-ura4+ cbp1Δ::kanMX6	$1.14 \times 10^{-5} \pm 1.32 \times 10^{-6}$
pfl10:3'kan-ura4+ cbp1Δ::kanMX6	$1.61 \times 10^{-5} \pm 3.19 \times 10^{-6}$
pfl10:ura4+-5'kan tf2-3Δ::kanMX6	$2.16 \times 10^{-5} \pm 1.03 \times 10^{-5}$
pfl5:3'kan-ura4+ kms1Δ::natMX6	$2.39 \times 10^{-5} \pm 9.35 \times 10^{-6}$
pfl5:3'kan-ura4+ kms1Δ::natMX6 cbp1Δ::kanMX6	$4.73 \times 10^{-5} \pm 1.82 \times 10^{-5}$
Intergenic recombination	
Genotype	**Rate of recombination**
pfl10:ura4+-5'kan pfl4:3'kan-ura4+	$2.09 \times 10^{-8} \pm 5.61 \times 10^{-9}$
pfl10:ura4-5'kan pfl4:3'kan-ura4 kms1Δ::hygMX6	$6.24 \times 10^{-8} \pm 1.45 \times 10^{-8}$
pfl10:ura4-5'kan pfl4:3'kan-ura4 cbp1Δ::hygMX6	$6.03 \times 10^{-8} \pm 3.98 \times 10^{-8}$
Repair of incompatible ends and loss of functional *ura4*	
Genotype	**Rate of repair**
mmf1:HOcs-ura4+-HOcs	$1.27 \times 10^{-6} \pm 3.27 \times 10^{-6}$
mmf1:HOcs-ura4+-HOcs lig4Δ::natMX6	$6.78 \times 10^{-7} \pm 1.37 \times 10^{-7}$
mmf1:HOcs-ura4+-HOcs pku70Δ::natMX6	$1.36 \times 10^{-6} \pm 8.10 \times 10^{-6}$
mmf1:HOcs-ura4+-HOcs kms1Δ::natMX6	$3.84 \times 10^{-6} \pm 4.24 \times 10^{-6}$

Table 1: Rates of recombination for the indicated genotypes in the repair assays used in this study. Rates are listed as mean ± standard deviation.

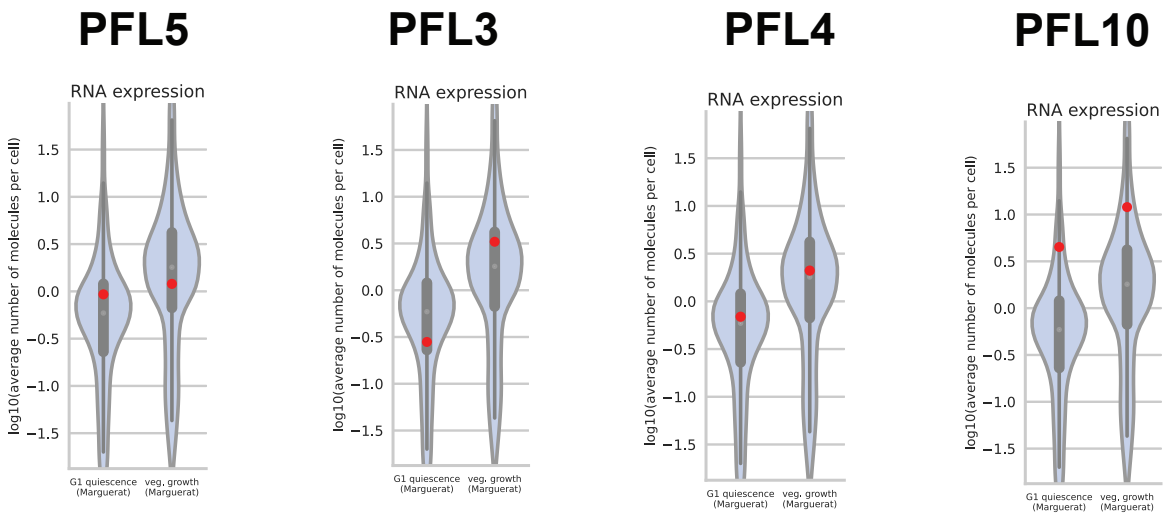

Supplemental Figure 1. *Pfl* genes are expressed. Data from a previous study (Marguerat et al., 2012) shows that *pfl*5, *pfl*3, *pfl*4, and *pfl*10 are expressed at a level at or above that of the average gene during the vegetative growth phase.

SPAPB2C8.01- *pfl*10 Amino acid sequence

Repeat #	Sequence
1	NTITTTLYSGSLEFTTTLDSANGTTPATIEVVEPAA
2	GTVTTTIYSGTTPFNTTLASATDTVPGTVEVVEPEA
3	GTVTTTVYSGTQEYTTTLATASGTVSGTVEVVDTAA
4	GTVTTTIYSGTTPFNTTLASATDTVPGTVEVVEPEA
5	GTVTTTVYSGTQEYTTTLATASGTVSGTVEVVDTAA
6	GTVTTTIYSGTTPFNTTLASATDTVPGTVEVVEPEA
7	GTVTTTVYSGTQEYTTTLATASGTVSGTVEVVDTAA
8	GTVTTTIYSGTTPFNTTLASATDTVPGTVEVVEPEA
9	GTVTTTVYSGTQEYTTTLATASGTVSGTVEVVDTAA
10	GTVTTTIYSGTTPFNTTLASATDTVPGTVEVVEPEA
11	GTVTTTVYSGTQEYTTTLATASGTVSGTVEVVDTAA
12	GTVTTTIYSGTTPFNTTLASATDTVPGTVEVVEPEA
13	GTVTTTVYSGTQEYTTTLATASGTVSGTVEVVDTAA
14	GTVTTTIYSGTTPFNTTLASATDTVPGTVEVVEPEA
15	GTVTTTVYSGTQEYTTTLATASGTVSGTVEVIEPAA
16	GTVTTTVYSGTQEYTTTLATASGTVSGTVEVIEPAA
17	GTVTSTVYSGTQEYTTTLATASGTVSGTVEVIEPAA
18	GTVTTTVYSGTQEYTTTLATASGTVSGTVEVIEPAA
19	GTVTTTVYSGSEVYTTTLASASESVPGTVEVVDPEA
20	GSVTTTIYSGSVEYTTVLADASGSVTGTVEVVEPAA
21	GTVTTTVYSGSEVYTTTLASASESVPGTVEVVDPEA
22	GSVTTTIYSGSVEYTTVLADASGSVTGTVEVVEPAA
23	GTVTGTLTSGSQFFTTTIAQASGSVSGNVEVIEPSG
24	STVTSTIYSGSESFTTTLAVGSGTIPGTVEVILPAP

SPCC188.09C- *pfl*4 Amino acid sequence

Repeat #	Sequence
1	STIYTTINSGTVASTYTVTLADGDV--VVKDIEPTA
2	GTVTTTITSGSHEFTTTLAEASGTVPGTVEVVEPLA
3	GTVTTTIHSGSVEYNTTLATASGTVPGTVEVVEPAV
4	GTVTTTIYSGSEEFTTTLASASGSISGTVEVIEPTA
5	GTVTTTIYSGDQEYTTILAEASGTVPGTVEVIEPAV
6	GTVTTTTYSGSVEYTTTLVPASGSVSGTVEVVEPAV
7	GTVTTTLQSGSQAFTTTV-PASGSVSGTVEVVQPTG
8	GTVTNTVYEGSQTITSTLATASGTVPGTVEVILPGP
9	STIY----SGTVATTITYDVSSTPASTVVV-I-PTA

SPBC1289.15-*pfl*5 Amino acid sequence

Repeat #	Sequence
1	GTITETIVSGSVGYTSTFPASGTTSGTVEVVEPTA
2	GTITETIVSGSVGYTSTFPANGTTSGTVEVVEPTA
3	GTITETIVSGSVGYTSTFPANGTTSGTVEVVEPTA
4	GTITETIVSGSVGYTSTFPANGTTSGTVEVVEPTA
5	GTVTETIVSGSVGYTSTFPASGTTSGTVEVVEPTA
6	GTITETIVSGSKAFTSTFPANGTTSGTVEVVEPTA
7	GTITKTIVSGSKTFTSTFPANGTTSGTVEVVEPTA
8	GTITETIVSGSVGYTSTFPANGTTSGTVEVVEPTA
9	GTITETIVSGSKTFTSTFPASGTTSGTVEVVEPTA
10	GTITETIVSGSKAFTSTFPANGTTSGTVEVVEPTA
11	GTITETIVSGSVGYTSTFPASGTTSGTVEVVEPTA
12	GTVTETIVSGSVGYTSTFPASGTTSGTVEVVEPTA
13	GTVTETIVSGSVGYTSTFPASGTTSGTVEVVEPTA
14	GTITETIVSGSKAFTSTFPANGTTSGTVEVVEPTA
15	GTITETIVSGSKTFTSTFPANGTTSGTVEVVEPTA
16	GTITETIVSGSVGYTSTFPASGTTSGTVEVVEPTA
17	GTVTETVISGSVSFMSTITAHDTSSGAVIVVEPTA
18	GTVTETIVSGSIPFTSTIPAQGTTSGTVEVVEPTA
19	GTVTETIISGSVGYTSTFPAQGTTSGTVEVVEPTA
20	GTVTETIISGSVGYTSTFPAQGTTSGTVEIVAPTA
21	GTVTETIVSGSIPFTSTIPAQGTTSGTVEVVEPTA
22	GTVTETIISGSVGYTSTFPAQGTTSGTVEIVAPTA
23	GTVTETIVSGSIPFTSTIPAQGTTSGTVEVVEPTA
24	GTVTETIISGSVGYTSTFPAQGTTSGTVEVVEPTA
25	GTVTETIVSGSIPFTSTIPAQGTTSGTVEIVVPTA
26	GTVTSTTGSGTSWFTTTVPATGTRSGSVIVVSPTA

SPBC947.04-*pfl*3 Amino acid sequence

Repeat #	Sequence
1	GTITLTTISGSDLYTSTFPANGTTSGTVEVVIPTA
2	GTVTETAVSGSELYTSTFPANGTTSGTVEVVIPTA
3	GTRTVTKISGSKFFTTTTDASGTVSGTVEVVLPTA
4	GTNTMTVVSGSRFFTSVVSASGTVSGEQVIVYPTA
5	GMVTETIVSGSEIFNTTYPASGTRTGTVEVVIPTA
6	GTVTETEISGSELYTSTFPANGTTSGTVEVVIPTA
7	GTRTVTKISGSKFFTTTTDASGTVSGTVEVVLPTA
8	GTNTMTVVSGSRFFTSVVSASGTVSGEHIIVEPTA
9	GVVTETVVSGSVGYTTTYPAHDTVSGTVEVVEPTA
10	GVVTETVVSGSVGYTTAYPAHDTVSGTVEVVEPTA
11	GVVTETVVSGSVGYTTTYPAHDTVSGTVEVVEPTA
12	GVVTETVVSGSVGYTTTYPAHDTVSGTVEVVEPTA
13	GVVTETVVSGSVGYTTTYPAHDTVSGTVEVVEPTA
14	GVVTETVVSGSVGYTTTYPAHDTVSGTVEVVEPTA
15	GVVTETVVSGSVGYTTTYPAHDTVSGTVEVVEPTA
16	GVVTETVVSGSVGYTTTYPAHDTVSGTVEVVEPTA
17	GVVTETVVSGSVGYTTTYPVQGTVSGTVMIVEPTA

Supplemental Figure 2. *Pfl* genes are repetitive and share sequence homology to each other. Alignment of the amino acid sequence of *pfl*10, *pfl*4, *pfl*5, and *pfl*3 demonstrate that not only are these genes repetitive, but they also share homology to each other.

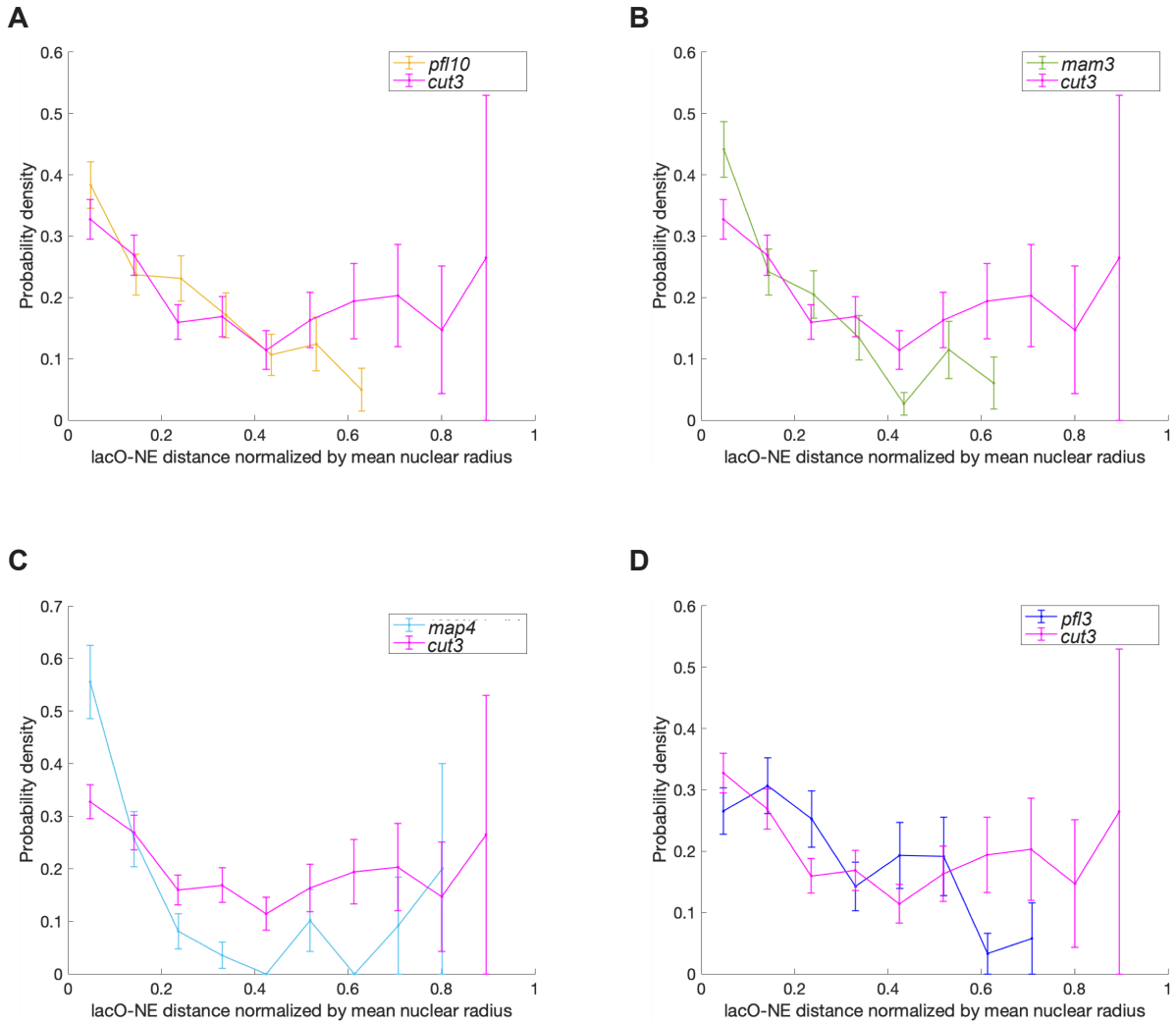

Supplemental Figure 3. A subset of *pfl* family genes are enriched at the nuclear periphery, unlike a generic locus, *cut3*. A probability density analysis shows that: a) *pfl10*, b) *mam3*, c) *map4*, and d) *pfl3* prefer to reside close to the nuclear periphery, unlike the generic locus *cut3*.

SPAPB2C8.01- *pfl10* Nucleotide sequence

	Sequence
1	AATACAATAACGACTACTCTTTATTCTGGTAGTCTCGAGTTTACTACTACTCTTGACTCGGCAAATGGGACTACCCCTGCAACCATTGAAGTAGTTGAACCTGCGGCA
2	GGGACCGTTACCACTACAATTTACTCTGGAACTACACCATTTAACACAACGCTTGCTTCCGCAACTGATACTGTTCCTGGCACTGTTGAGGTAGTTGAGCCTGAAGCT
3	GGAACTGTCACTACTACTGTATATTCTGGCACTCAAGAGTACACCACAACGCTTGCTACAGCCAGTGGTACTGTTTCAGGCACTGTTGAAGTAGTGGATACAGCAGCT
4	GGAACTGTTACTACTACAATTTACTCTGGAACTACACCATTTAACACAACGCTTGCTTCCGCAACTGATACTGTTCCTGGCACTGTTGAGGTAGTTGAGCCTGAAGCT
5	GGAACTGTCACTACTACTGTCTATTCTGGTACTCAAGAGTACACTACCACACTTGCTACAGCCAGTGGTACTGTTTCAGGCACTGTTGAAGTAGTGGATACAGCAGCT
6	GGAACTGTTACTACTACAATTTACTCTGGAACTACACCATTTAACACAACGCTTGCTTCCGCAACTGATACTGTTCCTGGCACTGTTGAGGTAGTTGAGCCTGAAGCT
7	GGAACTGTCACTACTACTGTATATTCTGGCACTCAAGAGTACACTACCACACTTGCTACAGCCAGTGGTACTGTTTCAGGCACTGTTGAAGTAGTGGATACAGCAGCT
8	GGAACTGTTACTACTACAATTTACTCTGGAACTACACCATTTAACACAACGCTTGCTTCCGCAACTGATACTGTTCCTGGCACTGTTGAGGTAGTTGAGCCTGAAGCT
9	GGAACTGTCACTACTACTGTCTATTCTGGTACTCAAGAGTACACTACCACACTTGCTACAGCCAGTGGTACTGTTTCAGGCACTGTTGAAGTAGTGGATACAGCAGCT
10	GGAACTGTTACTACTACAATTTACTCTGGAACTACACCATTCAACACAACACTTGCTTCCGCAACTGATACTGTTCCTGGCACTGTTGAGGTAGTTGAGCCTGAAGCT
11	GGAACTGTCACTACTACTGTATATTCTGGCACTCAAGAGTACACCACAACGCTTGCTACAGCTAGTGGTACTGTTTCAGGCACTGTTGAAGTAGTGGATACAGCAGCT
12	GGAACTGTTACTACTACAATTTACTCTGGAACTACACCATTCAACACAACACTTGCTTCCGCAACTGATACTGTTCCTGGCACTGTTGAGGTAGTTGAGCCTGAAGCT
13	GGAACTGTCACTACTACTGTCTATTCTGGTACTCAAGAGTACACCACAACGCTTGCTACAGCTAGTGGTACTGTTTCAGGCACTGTTGAAGTAGTGGATACAGCAGCT
14	GGAACTGTTACTACTACAATTTACTCTGGAACTACACCATTTAACACAACGCTTGCTTCCGCAACTGATACTGTTCCTGGCACTGTTGAGGTAGTTGAGCCTGAAGCT
15	GGAACTGTCACTACTACTGTATATTCTGGCACTCAAGAGTACACTACCACACTTGCTACAGCCAGTGGTACTGTTTCAGGTACCGTTGAAGTAATTGAACCTGCTGCA
16	GGAACCGTCACTACTACTGTATATTCTGGCACTCAAGAGTACACCACAACGCTTGCTACAGCCAGTGGTACTGTTTCAGGTACCGTTGAAGTAATTGAACCTGCTGCA
17	GGAACCGTTACTAGTACTGTCTATTCTGGTACTCAAGAGTACACCACAACGCTTGCTACAGCCAGTGGTACTGTTTCAGGCACCGTTGAAGTAATTGAACCCGCTGCA
18	GGAACCGTTACTACTACTGTTTACTCTGGTACTCAAGAGTACACTACCACACTTGCTACAGCCAGTGGTACTGTTTCAGGCACCGTTGAAGTAATTGAACCCGCTGCA
19	GGAACCGTTACTACTACTGTCTATTCTGGTAGCGAGGTATATACTACAACTCTCGCTTCTGCTTCCCGAATCTGTCCCCGGAACTGTTGAAGTAGTAGACCCAGAAGCT
20	GGAAGTGTCACCACTACTATCTATTCTGGTAGCGTAGAGTACACTACTGTTCTTGCTGATGCAAGTGGATCTGTTACTGGGACTGTTGAAGTTGTTGAACCGGCTGCA
21	GGAACTGTCACCACTACTGTTTACTCTGGTAGCGAGGTATATACTACAACTCTTGCTTCTGCTTCCCGAATCTGTCCCCGGAACTGTTGAAGTAGTAGACCCAGAAGCT
22	GGAAGTGTCACCACTACTATCTATTCTGGTAGCGTAGAGTACACTACTGTTCTTGCTGATGCAAGTGGATCTGTTACTGGAACTGTTGAAGTAGTTGAACCTGCTGCT
23	GGAACTGTTACCGGTACCCTCACTTCCGGTTCTCAGTTTTTTACTACTACTATCGCTCAAGCTAGTGGTTCCGTATCCGGCAACGTGGAGGTAATTGAGCCTTCTGGT
24	TCAACTGTTACTTCAACTATCTATAGTGGTAGTGAATCTTTCACTACGACTCTTGCTGTTGGAAGTGGAACTATTCCAGGTACTGTGGAGGTAATTCTCCCCGCTCCT

SPCC188.09C- *pfl4* Nucleotide sequence

	Sequence
1	AGCACAATATACACCACAATCAACAGCGGTACTGTAGCTTCCACATATACTGTCACACTGGCAGATGGCGACGTT------GTGGTCAAAGACATAGAGCCCACTGCA
2	GGAACGGTGACTACCACGATCACTTCAGGTAGTCACGAGTTCACTACCACTCTTGCTGAAGCCAGTGGTACTGTCCCTGGAACGGTTGAGGTAGTTGAGCCTCTAGCT
3	GGAACTGTTACTACTACTATTCATTCCGGTAGTGTAGAATACAACACCACTCTTGCTACCGCAAGTGGAACTGTTCCTGGTACCGTTGAGGTTGTTGAACCCGCTGTT
4	GGAACTGTTACTACTACCATATACTCAGGCAGTGAAGAGTTTACAACTACTTTGGCATCTGCCTCTGGTTCAATTTCAGGTACCGTTGAAGTAATTGAACCTACAGCT
5	GGCACAGTAACTACCACTATTTACTCTGGCGACCAAGAGTATACCACTATCCTTGCTGAAGCCAGTGGAACTGTTCCAGGTACTGTTGAAGTGATTGAACCTGCTGTT

6	GGAACCGTTACGACCACTACTTACTCAGGTAGTGTAGAGTATACAACTACTTTGGTACCTGCCTCTGGTTCTGTCTCCGGAACCGTTGAGGTCGTTGAGCCTGCGGTT
7	GGAACTGTGACGACGACATTGCAGTCTGGGTCTCAAGCCTTTACAACCACTGTG---CCCGCCTCCGGTAGTGTATCGGGAACTGTTGAGGTAGTTCAGCCAACTGGT
8	GGCACTGTTACTAATACAGTATATGAGGGATCTCAGACCATTACTTCGACTCTTGCAACAGCTAGTGGTACTGTTCCAGGTACTGTTGAAGTTATTCTTCCTGGGCCT
9	AGCACAATCTAT----------TCGGGAACTGTTGCTACCACTATTACATATGATGTTTCTAGTACGCCTGCGTCTACTGTTGTTGTT---ATC---CCTACTGCT

Supplemental Figure 4. An alignment of the nucleotide sequences of *pfl*10 and *pfl*4 shows their homolog

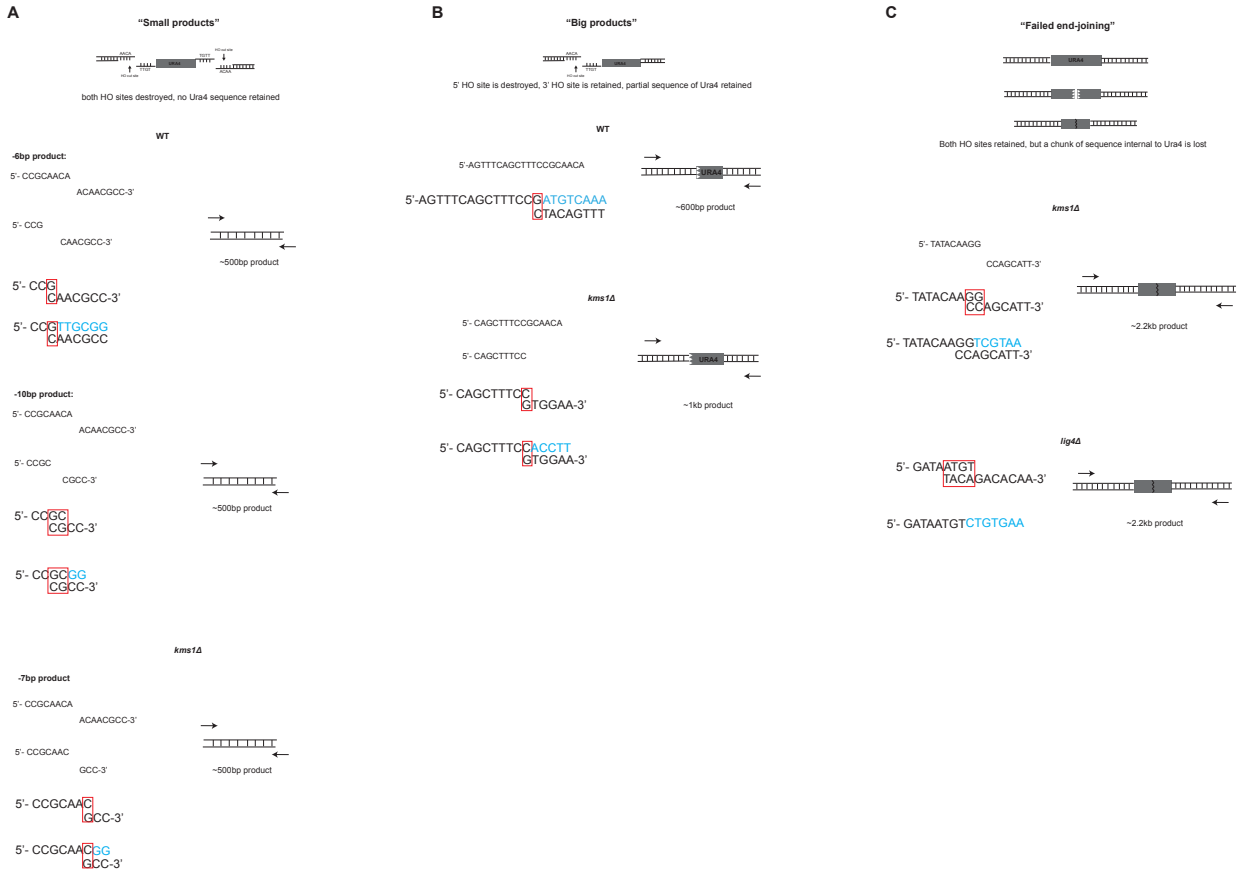

Supplemental Figure 5. Recombinants can maintain portions of *ura4* by repairing with microhomologies within the *ura4* coding sequence. A) "Small products" are individual FOA+ products where both HO sites are destroyed. These products are outlined in Figure 7D. Two of the WT products (the -6bp product and the -10bp product) are possible via rejoining of a 1-2bp microhomology. One *kms1Δ* product (the -7bp product) is also a possible via a 1bp microhomology. B) "Big products" are products where the HO site 5' to *ura4* is destroyed, but the HO site 3' to *ura4* is retained. These are possible via repair by a 1bp microhomology within the *ura4* coding sequence. Interestingly, the product size in WT is similar to the dual cutters, making it difficult to distinguish between them in an ensemble of FOA+ colonies, as in Fig. 7C. In *kms1Δ* cells we observe many examples that retain more of the sequence, which explains the variety of product sizes seen in Fig. 7C. C) "Failed cNHEJ" products have both HO sites intact, are not observed in WT cells, and arise in cells lacking *lig4*, suggesting that they are unable to complete cNHEJ. These examples lost ~300bp of sequence internal to *ura4* (resulting in a ~2.2kb product), and the junction is a result of rejoining of microhomologies. Similar products are observed in *kms1Δ* cells where repair appears to occur via a 2bp microhomology.

Table S1

Strains used in this study

Strain	Genotype
MKSP1019	*h- ade6? ura4-D18 leu? sad1-mCherry:kanMX6 rad52-GFP:kanMX6*
MKSP1184	*h- ade? ura4-D18 leu? sad1-mCherry:kanMX6 rad552-GFP:kanMX6 kms1Δ::hygMX6*
MKSP1615	*h- ade6-M216 ura4-D18 leu1-32 pfl10:ura4+-5'kanMX6 pfl4:3'kanMX6-ura4+*
MKSP1616	*h+ ade6-M216 ura4-D18 leu1-32 pfl10:ura4+-5'kanMX6 pfl4:3'kanMX6-ura4+ kms1Δ::hygMX6*
MKSP1652	*h+ ade6-M216 ura4-D18 leu1-32 pfl5:ura4+-5'kan*
MKSP1655	*h? ade6-M216 ura4-D18 leu1-32 pfl5:3'kan-ura4+ cbp1Δ::kanMX6*
MKSP1661	*h- pfl5:lacO-ura4+ lacI-GFP cut11-mCherry:natMX6*
MKSP1663	*h? pfl10:lacO-ura4+ lacI-GFP cut11-mCherry:natMX6*
MKSP1668	*h? pfl10:lacO-ura4+ lacI-GFP cut11-mCherry:natMX6 cbp1Δ::hygMX6*
MKSP1713	*h? ade6-M216 ura4-D18 leu1-32 pfl10:ura4+-5'kan pfl4:3'kan-ura4 cbp1Δ::hygMX6*
MKSP1714	*h- ade6-M216 ura4-D18 leu1-32 pfl3:3'kan-ura4+*
MKSP1838	*h- mam3:lacO-ura4+ lacI-GFP cut11-mCherry:natMX6*
MKSP1839	*h+ ade6-M216 ura4-D18 leu1-32 pfl10:ura4+-5'kan tf2-3Δ::kanMX6*
MKSP1841	*h? ade6-M216 ura4-D18 leu1-32 pfl5:3'kan-ura4+ lig4Δ::kanMX6*
MKSP1855	*h? ade6-M216 ura4-D18 leu1-32 pfl5:ura4+-5'kan exo1Δ::kanMX6*
MKSP1858	*h? ade6-M216 ura4-D18 leu1-32 pfl5:ura4+-5'kan rad52Δ::kanMX6*
MKSP1880	*h- ade6-M216 ura4-D18 leu1-32 pfl3:3'kan-ura4+ cbp1Δ::kanMX6*
MKSP1882	*h- ade6-M216 ura4-D18 leu1-32 pfl10:3'kan-ura4+*
MKSP1884	*h? ade6-M216 ura4-D18 leu1-32 pfl5:ura4+-5'kan swi10Δ::kanMX6*
MKSP1888	*h? ade6-M216 ura4-D18 leu1-32 pfl5:ura4+-5'kan rad51Δ::hygMX6*
MKSP1895	*h? ade6-M216 ura4-D18 leu1-32 pfl10:3'kan-ura4+ cbp1Δ::kanMX6*
MKSP1938	*h- map4:lacO-ura4+ lacI-GFP cut11-mCherry:natMX6*
MKSP1944	*h+ ade6-M216 ura4-D18 leu1-32 pfl5:ura4+-5'kan rad55Δ::hygMX6*
MKSP1966	*h+ ade6-M216 ura4-D18 leu1-32 map4 200-3:ura4+-5'kan*
MKSP1974	*h- ade6-M216 ura4-D18 leu1-32 mam3 201-1:3'kan-ura4+*
MKSP1983	*h? pfl5:lacO-ura4+ lacI-GFP cut11-mCherry:natMX6 cbp1Δ::kanMX6*
MKSP2018	*h- leu1-32 ura4-D18 ade6? lys1? his7::GFP-LacI-NLS-his7 cut3-477::lacO-cut3+ cut11-mCherry::natR*
MKSP2310	*h- pfl3:lacO-ura4+ lacI-GFP cut11-mCherry:natMX6*
MKSP2354	*h? pfl3:lacO-ura4+ lacI-GFP cut11-mCherry:natMX6 cbp1Δ::kanMX6*
MKSP3795	*h- ade6? ura4-D18 leu? sad1-mCherry:kanMX6 rad52-GFP:kanMX6 rad51Δ::HygMX6*
MKSP3796	*h- ade6? ura4-D18 leu? sad1-mCherry:kanMX6 rad52-GFP:kanMX6 rad51Δ::HygMX6 kms1Δ:: HygR*
MKSP4299	*h- ade6+ leu1-32 ura4-D18 mmf1-HOcs-ura4+-HOcs*
MKSP4305	*h- ade6+ leu1-32 ura4-D18 mmf1-HOcs-ura4+-HOcs kms1Δ::natMX6*

MKSP4313	*h- ade6+ leu1-32 ura4-D18 mmf1-HOcs-ura4+-HOcs lig4Δ::natMX6*
MKSP4362	*h- ade6+ leu1-32 ura4-D18 mmf1-HOcs-ura4+-HOcs pku70Δ::natMX6*
MKSP4434	*h? ade6-M216 ura4-D18 leu1-32 pfl5:3'kan-ura4+ kms1Δ::natMX6*
MKSP4435	*h? ade6-M216 ura4-D18 leu1-32 pfl5:3'kan-ura4+ kms1Δ::natMX6 cbp1Δ::kanMX6*

Note: precise insertion sites of the *ura4* and *kanR* cassette fragments are uncertain due to the repetitive nature of the *pfl* genes. For approximate locations please see Table S2.

Table S2

Insertion sites

Genetic locus	LacO insertion location
cut3	chrII:1006688-1002263
pfl5	chrII; 4403547-4403553
pfl10	chrI; 2959337-2961046
pfl3	chrII; 665084-667124
mam3	chrI; 1837071- 1838471
map4	chrII; 2450913-2452027

Genetic locus	Approximate *ura4* insertion location
pfl5	chrII; 4421537-4424856
pfl10	chrI; 2959337-2961046
pfl3	chrII; 665084-667124
mam3	chrI; 1837071- 1838471
map4	chrII; 2450913-2452027

For the approximation of *ura4* insertions sites within the repeats of the *pfl* genes we have determined approximate locations based on PCR analysis.

Table S3

Primers used in this study

Primer name	Sequence
Mam3_For	5'-TGGTTCCGTTGGATTTACC-3'
Mam3_Rev	5'-CAGAATGGTGAGGTGTTCC-3'
Map4_For	5'- GTGTCTTCATCTCATCCGTATC-3'
Map4_Rev	5'- TATCGTCCTGGTCCAACCT-3'
PFL5_For	5'- CCACACTCAACAATAAGCACTC-3'
PFL5_Rev	5'- GCGGGAACAGTAGTAGTAAACC-3'
PFL3_For	5'- TAGTGGAACAGTCAGCGGT -3'
PFL3_Rev	5'- CAGCCAGGGAATAAAGAAGG -3'
PFL10For	5'- ACTCTTGACTCGGCAAATG-3'
PFL10Rev	5'- AACAGTTGAACCAGAAGGCT-3'
PFL4For	5'- TGTGGTCAAAGACATAGAGCC-3'
PFL4Rev	5'- GGATAACAACAACAGTAGACGC-3'
Mmf1_L1	5'- GCATTTTGTCGATGATGAACGTTG-3'
Mmf1_L1Seq	5'- CGGTTGGATACATCTCTGTCATC-3'
Mmf1_L6	5'- GGCGCTTTTCATTTTCGTGC-3'
Aly3F	5'- CGTGTTATTAGGACTATTCCTC-3'
Aly3R	5'- CCTACGTAGCAGTAAGAATACAGC-3'
Ura4_ins_AscI	5'-CAGTCAGGCGCGCCAGCTTAGCTACAAATCCCACTG-3'
Ura4_ins_PmeI	5'- CTGACAGTTTAAACGGTCGACGGTATCGATAAGC-3'
Ura_int_chk	5'- GCCAGCTGAAGCTTCGTAC-3'
HOcs_ins_AscI_F	5'-TTGGCGCGCCAGTTTCAGCTTTCCGCAACAGTATAATTTTATAAAGGCGCGCCTT-3'
HO_ins_AscI_R	5'-AAGGCGCGCCTTTATAAAATTATACTGTTGCGGAAAGCTGAAACTGGCGCGCCAA-3'

Table S4

Plasmids used in this study

Plasmid name	Method of generation	Description
pSR10_ura4_5.6kb	Previous work (Leland & King, 2014)	Integrated nearby the *pfl* loci and *cut3* to visualize their localization within then nucleus
pFA6a_HOcs_Ura	Plasmid was cut at AscI and PmeI to release the Hyg-resistance gene fragment. An insert with the *S. pombe ura4* gene was created by amplifying *ura4* from a pFA6a-Ura4.	Used plasmid from a previous study (Leland et al., 2018) which contained a modified MX6-based hygromycin-resistance cassette containing the HO cut site to switch the marker from hygromycin to *ura4*.
pFA6a_HOcs_Ura_HOcs	Added another HO endonuclease cut site to at the AscI site of pFA6a_HOcs_Ura. Care was taken to ensure proper orientation of the cut sites.	Integrated into the *mmf1* locus of *S. pombe* for the salvage DNA repair assay.

References

Ahmed, S., Brickner, D. G., Light, W. H., Cajigas, I., McDonough, M., Froyshteter, A. B., Volpe, T., & Brickner, J. H. (2010). DNA zip codes control an ancient mechanism for gene targeting to the nuclear periphery. *Nature Cell Biology*, *12*(2), 111-118. https://doi.org/10.1038/ncb2011

Ahmed, S., & Brickner, J. H. (2007). Regulation and epigenetic control of transcription at the nuclear periphery. *Trends in Genetics*, *23*(8), 396-402. https://doi.org/https://doi.org/10.1016/j.tig.2007.05.009

Amaral, N., Ryu, T., Li, X., & Chiolo, I. (2017). Nuclear Dynamics of Heterochromatin Repair. *Trends in Genetics*, *33*(2), 86-100. https://doi.org/10.1016/j.tig.2016.12.004

Anand, R. P., Tsaponina, O., Greenwell, P. W., Lee, C.-S., Du, W., Petes, T. D., & Haber, J. E. (2014). Chromosome rearrangements via template switching between diverged repeated sequences. *Genes & Development*, *28*(21), 2394-2406. https://doi.org/10.1101/gad.250258.114

Bähler, J., Wu, J. Q., Longtine, M. S., Shah, N. G., McKenzie, A., 3rd, Steever, A. B., Wach, A., Philippsen, P., & Pringle, J. R. (1998). Heterologous modules for efficient and versatile PCR-based gene targeting in Schizosaccharomyces pombe. *Yeast*, *14*(10), 943-951. https://doi.org/10.1002/(sici)1097-0061(199807)14:10<943::Aid-yea292>3.0.Co;2-y

Berti, M., Teloni, F., Mijic, S., Ursich, S., Fuchs, J., Palumbieri, M. D., Krietsch, J., Schmid, J. A., Garcin, E. B., Gon, S., Modesti, M., Altmeyer, M., & Lopes, M. (2020). Sequential role of RAD51 paralog complexes in replication fork remodeling and restart. *Nature Communications*, *11*(1), 3531. https://doi.org/10.1038/s41467-020-17324-z

Biehs, R., Steinlage, M., Barton, O., Juhász, S., Künzel, J., Spies, J., Shibata, A., Jeggo, P. A., & Löbrich, M. (2017). DNA Double-Strand Break Resection Occurs during Non-homologous End Joining in G1 but Is Distinct from Resection during Homologous Recombination. *Molecular Cell*, *65*(4), 671-684.e675. https://doi.org/10.1016/j.molcel.2016.12.016

Bonilla, B., Hengel, S. R., Grundy, M. K., & Bernstein, K. A. (2020). RAD51 Gene Family Structure and Function. *Annu Rev Genet*, *54*, 25-46. https://doi.org/10.1146/annurev-genet-021920-092410

Branzei, D., & Foiani, M. (2008). Regulation of DNA repair throughout the cell cycle. *Nature Reviews Molecular Cell Biology*, *9*(4), 297-308. https://doi.org/10.1038/nrm2351

Brickner, J. H., & Walter, P. (2004). Gene Recruitment of the Activated INO1 Locus to the Nuclear Membrane. *PLOS Biology*, *2*(11), e342. https://doi.org/10.1371/journal.pbio.0020342

Cam, H. P., Noma, K., Ebina, H., Levin, H. L., & Grewal, S. I. (2008). Host genome surveillance for retrotransposons by transposon-derived proteins. *Nature*, *451*(7177), 431-436. https://doi.org/10.1038/nature06499

Cannan, W. J., & Pederson, D. S. (2016). Mechanisms and Consequences of Double-Strand DNA Break Formation in Chromatin. *J Cell Physiol*, *231*(1), 3-14. https://doi.org/10.1002/jcp.25048

Capella, M., Mandemaker, I. K., Martín Caballero, L., den Brave, F., Pfander, B., Ladurner, A. G., Jentsch, S., & Braun, S. (2021). Nucleolar release of rDNA repeats for repair involves SUMO-mediated untethering by the Cdc48/p97 segregase. *Nature Communications*, *12*(1), 4918. https://doi.org/10.1038/s41467-021-25205-2

Caridi, P. C., Delabaere, L., Zapotoczny, G., & Chiolo, I. (2017). And yet, it moves: nuclear and chromatin dynamics of a heterochromatic double-strand break. *Philosophical Transactions of the Royal Society B: Biological Sciences*, *372*(1731), 20160291. https://doi.org/doi:10.1098/rstb.2016.0291

Casolari, J. M., Brown, C. R., Komili, S., West, J., Hieronymus, H., & Silver, P. A. (2004). Genome-wide localization of the nuclear transport machinery couples transcriptional status and nuclear organization. *Cell*, *117*(4), 427-439. https://doi.org/10.1016/s0092-8674(04)00448-9

Chen, M., & Gartenberg, M. R. (2014). Coordination of tRNA transcription with export at nuclear pore complexes in budding yeast. *Genes & Development*, *28*(9), 959-970. https://doi.org/10.1101/gad.236729.113

Chen, Z., & Tyler, J. K. (2022). The Chromatin Landscape Channels DNA Double-Strand Breaks to Distinct Repair Pathways. *Front Cell Dev Biol*, *10*, 909696. https://doi.org/10.3389/fcell.2022.909696

Chiolo, I., Altmeyer, M., Legube, G., & Mekhail, K. (2025). Nuclear and genome dynamics underlying DNA double-strand break repair. *Nat Rev Mol Cell Biol*. https://doi.org/10.1038/s41580-025-00828-1

Chiolo, I., Minoda, A., Colmenares, Serafin U., Polyzos, A., Costes, Sylvain V., & Karpen, Gary H. (2011). Double-Strand Breaks in Heterochromatin Move Outside of a Dynamic HP1a Domain to Complete Recombinational Repair. *Cell*, *144*(5), 732-744. https://doi.org/https://doi.org/10.1016/j.cell.2011.02.012

Choi, J., Kong, M., Gallagher, D. N., Li, K., Bronk, G., Cao, Y., Greene, E. C., & Haber, J. E. (2022). Repair of mismatched templates during Rad51-dependent Break-Induced Replication. *PLOS Genetics*, *18*(9), e1010056. https://doi.org/10.1371/journal.pgen.1010056

Churikov, D., Charifi, F., Eckert-Boulet, N., Silva, S., Simon, M. N., Lisby, M., & Géli, V. (2016). SUMO-Dependent Relocalization of Eroded Telomeres to Nuclear Pore Complexes Controls Telomere Recombination. *Cell Rep*, *15*(6), 1242-1253. https://doi.org/10.1016/j.celrep.2016.04.008

Conrad, M. N., Lee, C.-Y., Chao, G., Shinohara, M., Kosaka, H., Shinohara, A., Conchello, J. A., & Dresser, M. E. (2008). Rapid Telomere Movement in Meiotic Prophase Is Promoted By NDJ1, MPS3, and CSM4 and Is Modulated by Recombination. *Cell*, *133*(7), 1175-1187. https://doi.org/10.1016/j.cell.2008.04.047

Covo, S., Westmoreland, J. W., Gordenin, D. A., & Resnick, M. A. (2010). Cohesin Is limiting for the suppression of DNA damage-induced recombination between homologous chromosomes. *PLoS Genet*, *6*(7), e1001006. https://doi.org/10.1371/journal.pgen.1001006

Cranz-Mileva, S., Reilly, E., Chalhoub, N., Patel, R., Atanassova, T., Cao, W., Ellison, C., & Zaratiegui, M. (2024). Transposon Removal Reveals Their Adaptive Fitness Contribution. *Genome Biol Evol*, *16*(2). https://doi.org/10.1093/gbe/evae010

Daulny, A., Mejía-Ramírez, E., Reina, O., Rosado-Lugo, J., Aguilar-Arnal, L., Auer, H., Zaratiegui, M., & Azorin, F. (2016). The fission yeast CENP-B protein Abp1 prevents pervasive transcription of repetitive DNA elements. *Biochim Biophys Acta*, *1859*(10), 1314-1321. https://doi.org/10.1016/j.bbagrm.2016.06.009

Decottignies, A. (2007). Microhomology-mediated end joining in fission yeast is repressed by pku70 and relies on genes involved in homologous recombination. *Genetics*, *176*(3), 1403-1415. https://doi.org/10.1534/genetics.107.071621

DeGennaro, C. M., Alver, B. H., Marguerat, S., Stepanova, E., Davis, C. P., Bähler, J., Park, P. J., & Winston, F. (2013). Spt6 Regulates Intragenic and Antisense Transcription, Nucleosome Positioning, and Histone Modifications Genome-Wide in Fission Yeast. *Molecular and Cellular Biology*, *33*(24), 4779-4792. https://doi.org/10.1128/MCB.01068-13

Dong, W., Oya, E., Zahedi, Y., Prasad, P., Svensson, J. P., Lennartsson, A., Ekwall, K., & Durand-Dubief, M. (2020). Abo1 is required for the H3K9me2 to H3K9me3 transition in heterochromatin. *Sci Rep*, *10*(1), 6055. https://doi.org/10.1038/s41598-020-63209-y

Dumont, A., Mendiboure, N., Savocco, J., Anani, L., Moreau, P., Thierry, A., Modolo, L., Jost, D., & Piazza, A. (2024). Mechanism of homology search expansion during recombinational DNA break repair in Saccharomyces cerevisiae. *Molecular Cell*, *84*(17), 3237-3253.e3236. https://doi.org/10.1016/j.molcel.2024.08.003

Elbakry, A., & Löbrich, M. (2021). Homologous Recombination Subpathways: A Tangle to Resolve. *Front Genet*, *12*, 723847. https://doi.org/10.3389/fgene.2021.723847

Ellenberger, T., & Tomkinson, A. E. (2008). Eukaryotic DNA Ligases: Structural and Functional Insights. *Annual Review of Biochemistry*, *77*(Volume 77, 2008), 313-338. https://doi.org/https://doi.org/10.1146/annurev.biochem.77.061306.123941

Feng, G., Leem, Y.-E., & Levin, H. L. (2012). Transposon integration enhances expression of stress response genes. *Nucleic Acids Research*, *41*(2), 775-789. https://doi.org/10.1093/nar/gks1185

Ferreira, M. G., & Cooper, J. P. (2004). Two modes of DNA double-strand break repair are reciprocally regulated through the fission yeast cell cycle. *Genes & Development*, *18*(18), 2249-2254. https://doi.org/10.1101/gad.315804

Gallardo, P., Barrales, R. R., Daga, R. R., & Salas-Pino, S. (2019). Nuclear Mechanics in the Fission Yeast. *Cells*, *8*(10), 1285. https://www.mdpi.com/2073-4409/8/10/1285

Haber, J. E. (2018). DNA Repair: The Search for Homology. *BioEssays*, *40*(5), 1700229. https://doi.org/https://doi.org/10.1002/bies.201700229

Hashimoto, Y., Ray Chaudhuri, A., Lopes, M., & Costanzo, V. (2010). Rad51 protects nascent DNA from Mre11-dependent degradation and promotes continuous DNA synthesis. *Nature structural & molecular biology*, *17*(11), 1305-1311. https://doi.org/10.1038/nsmb.1927

Hastings, P. J., Lupski, J. R., Rosenberg, S. M., & Ira, G. (2009). Mechanisms of change in gene copy number. *Nature Reviews Genetics*, *10*(8), 551-564. https://doi.org/10.1038/nrg2593

Helleday, T., Lo, J., van Gent, D. C., & Engelward, B. P. (2007). DNA double-strand break repair: From mechanistic understanding to cancer treatment. *DNA Repair*, *6*(7), 923-935. https://doi.org/https://doi.org/10.1016/j.dnarep.2007.02.006

Hentges, P., Van Driessche, B., Tafforeau, L., Vandenhaute, J., & Carr, A. M. (2005). Three novel antibiotic marker cassettes for gene disruption and marker switching in Schizosaccharomyces pombe. *Yeast*, *22*(13), 1013-1019. https://doi.org/10.1002/yea.1291

Hoff, E. F., Levin, H. L., & Boeke, J. D. (1998). Schizosaccharomyces pombe retrotransposon Tf2 mobilizes primarily through homologous cDNA recombination. *Mol Cell Biol*, *18*(11), 6839-6852. https://doi.org/10.1128/mcb.18.11.6839

Horigome, C., Bustard, D. E., Marcomini, I., Delgoshaie, N., Tsai-Pflugfelder, M., Cobb, J. A., & Gasser, S. M. (2016). PolySUMOylation by Siz2 and Mms21 triggers relocation of DNA breaks to nuclear pores through the Slx5/Slx8 STUbL. *Genes Dev*, *30*(8), 931-945. https://doi.org/10.1101/gad.277665.116

Horigome, C., Oma, Y., Konishi, T., Schmid, R., Marcomini, I., Hauer, Michael H., Dion, V., Harata, M., & Gasser, Susan M. (2014). SWR1 and INO80 Chromatin Remodelers Contribute to DNA Double-Strand Break Perinuclear Anchorage Site Choice. *Molecular Cell*, *55*(4), 626-639. https://doi.org/https://doi.org/10.1016/j.molcel.2014.06.027

Horn, H. F., Kim, D. I., Wright, G. D., Wong, E. S., Stewart, C. L., Burke, B., & Roux, K. J. (2013). A mammalian KASH domain protein coupling meiotic chromosomes to the cytoskeleton. *J Cell Biol*, *202*(7), 1023-1039. https://doi.org/10.1083/jcb.201304004

Hustedt, N., & Durocher, D. (2016). The control of DNA repair by the cell cycle. *Nat Cell Biol*, *19*(1), 1-9. https://doi.org/10.1038/ncb3452

Iwasaki, O., Tanaka, A., Tanizawa, H., Grewal, S. I. S., & Noma, K.-i. (2010). Centromeric Localization of Dispersed Pol III Genes in Fission Yeast. *Molecular Biology of the Cell*, *21*(2), 254-265. https://doi.org/10.1091/mbc.e09-09-0790

Jeggo, P. A., & and Lobrich, M. (2005). Artemis links ATM to Double Strand Break Rejoining. *Cell Cycle*, *4*(3), 359-362. https://doi.org/10.4161/cc.4.3.1527

Kalocsay, M., Hiller, N. J., & Jentsch, S. (2009). Chromosome-wide Rad51 spreading and SUMO-H2A.Z-dependent chromosome fixation in response to a persistent DNA double-strand break. *Mol Cell*, *33*(3), 335-343. https://doi.org/10.1016/j.molcel.2009.01.016

Kramarz, K., Schirmeisen, K., Boucherit, V., Ait Saada, A., Lovo, C., Palancade, B., Freudenreich, C., & Lambert, S. A. E. (2020). The nuclear pore primes recombination-dependent DNA synthesis at arrested forks by promoting SUMO removal. *Nature Communications*, *11*(1), 5643. https://doi.org/10.1038/s41467-020-19516-z

Krejci, L., Altmannova, V., Spirek, M., & Zhao, X. (2012). Homologous recombination and its regulation. *Nucleic Acids Research*, *40*(13), 5795-5818. https://doi.org/10.1093/nar/gks270

Kwon, E.-J. G., Laderoute, A., Chatfield-Reed, K., Vachon, L., Karagiannis, J., & Chua, G. (2012). Deciphering the Transcriptional-Regulatory Network of Flocculation in Schizosaccharomyces pombe. *PLOS Genetics*, *8*(12), e1003104. https://doi.org/10.1371/journal.pgen.1003104

Langerak, P., Mejia-Ramirez, E., Limbo, O., & Russell, P. (2011). Release of Ku and MRN from DNA Ends by Mre11 Nuclease Activity and Ctp1 Is Required for Homologous Recombination Repair of Double-Strand Breaks. *PLOS Genetics*, *7*(9), e1002271. https://doi.org/10.1371/journal.pgen.1002271

Lawrence, K. S., Tapley, E. C., Cruz, V. E., Li, Q., Aung, K., Hart, K. C., Schwartz, T. U., Starr, D. A., & Engebrecht, J. (2016). LINC complexes promote homologous recombination in part through inhibition of nonhomologous end joining. *Journal of Cell Biology*, *215*(6), 801-821. https://doi.org/10.1083/jcb.201604112

Lee, C. Y., Horn, H. F., Stewart, C. L., Burke, B., Bolcun-Filas, E., Schimenti, J. C., Dresser, M. E., & Pezza, R. J. (2015). Mechanism and regulation of rapid telomere prophase movements in mouse meiotic chromosomes. *Cell Rep*, *11*(4), 551-563. https://doi.org/10.1016/j.celrep.2015.03.045

Lee, K., & Lee, S. E. (2007). Saccharomyces cerevisiae Sae2- and Tel1-Dependent Single-Strand DNA Formation at DNA Break Promotes Microhomology-Mediated End Joining. *Genetics*, *176*(4), 2003-2014. https://doi.org/10.1534/genetics.107.076539

Leland, B. A., Chen, A. C., Zhao, A. Y., Wharton, R. C., & King, M. C. (2018). Rev7 and 53BP1/Crb2 prevent RecQ helicase-dependent hyper-resection of DNA double-strand breaks. *eLife*, *7*, e33402. https://doi.org/10.7554/eLife.33402

Leland, B. A., & King, M. C. (2014). Using LacO Arrays to Monitor DNA Double-Strand Break Dynamics in Live Schizosaccharomyces pombe Cells. In N. Wajapeyee (Ed.), *Cancer Genomics and Proteomics: Methods and Protocols* (pp. 127-141). Springer New York. https://doi.org/10.1007/978-1-4939-0992-6_11

Lemaître, C., Grabarz, A., Tsouroula, K., Andronov, L., Furst, A., Pankotai, T., Heyer, V., Rogier, M., Attwood, K. M., Kessler, P., Dellaire, G., Klaholz, B., Reina-San-Martin, B., & Soutoglou, E. (2014). Nuclear position dictates DNA repair pathway choice. *Genes Dev*, *28*(22), 2450-2463. https://doi.org/10.1101/gad.248369.114

Li, P., Li, J., Li, M., Dou, K., Zhang, M.-J., Suo, F., & Du, L.-L. (2012). Multiple end joining mechanisms repair a chromosomal DNA break in fission yeast. *DNA Repair*, *11*(2), 120-130. https://doi.org/https://doi.org/10.1016/j.dnarep.2011.10.011

Li, X., & Heyer, W.-D. (2008). Homologous recombination in DNA repair and DNA damage tolerance. *Cell Research*, *18*(1), 99-113. https://doi.org/10.1038/cr.2008.1

Linder, T., & Gustafsson, C. M. (2008). Molecular phylogenetics of ascomycotal adhesins—A novel family of putative cell-surface adhesive proteins in fission yeasts. *Fungal Genetics and Biology*, *45*(4), 485-497. https://doi.org/https://doi.org/10.1016/j.fgb.2007.08.002

Liu, Y., Zhang, H., Veeraraghavan, J., Bambara, R. A., & Freudenreich, C. H. (2004). Saccharomyces cerevisiae Flap Endonuclease 1 Uses Flap Equilibration To Maintain Triplet Repeat Stability. *Molecular and Cellular Biology*, *24*(9), 4049-4064. https://doi.org/10.1128/MCB.24.9.4049-4064.2004

Lorenz, D. R., Mikheyeva, I. V., Johansen, P., Meyer, L., Berg, A., Grewal, S. I. S., & Cam, H. P. (2012). CENP-B Cooperates with Set1 in Bidirectional Transcriptional Silencing and Genome Organization of Retrotransposons. *Molecular and Cellular Biology*, *32*(20), 4215-4225. https://doi.org/10.1128/MCB.00395-12

Lottersberger, F., Karssemeijer, R. A., Dimitrova, N., & de Lange, T. (2015). 53BP1 and the LINC Complex Promote Microtubule-Dependent DSB Mobility and DNA Repair. *Cell*, *163*(4), 880-893. https://doi.org/10.1016/j.cell.2015.09.057

Lu, H., Shamanna, R. A., de Freitas, J. K., Okur, M., Khadka, P., Kulikowicz, T., Holland, P. P., Tian, J., Croteau, D. L., Davis, A. J., & Bohr, V. A. (2017). Cell cycle-dependent phosphorylation regulates RECQL4 pathway choice and ubiquitination in DNA double-strand break repair. *Nature Communications*, *8*(1), 2039. https://doi.org/10.1038/s41467-017-02146-3

Ma, J. L., Kim, E. M., Haber, J. E., & Lee, S. E. (2003a). Yeast Mre11 and Rad1 proteins define a Ku-independent mechanism to repair double-strand breaks lacking overlapping end sequences. *Mol Cell Biol*, *23*(23), 8820-8828. https://doi.org/10.1128/mcb.23.23.8820-8828.2003

Ma, J. L., Kim, E. M., Haber, J. E., & Lee, S. E. (2003b). Yeast Mre11 and Rad1 Proteins Define a Ku-Independent Mechanism to Repair Double-Strand Breaks Lacking Overlapping End Sequences [Article]. *Molecular and Cellular Biology*, *23*(23), 8820-8828. https://doi.org/10.1128/MCB.23.23.8820-8828.2003

Manolis, K. G., Nimmo, E. R., Hartsuiker, E., Carr, A. M., Jeggo, P. A., & Allshire, R. C. (2001). Novel functional requirements for non‐homologous DNA end joining in Schizosaccharomyces pombe. *The EMBO journal*, *20*(1-2), 210-221-221. https://doi.org/https://doi.org/10.1093/emboj/20.1.210

Marguerat, S., Schmidt, A., Codlin, S., Chen, W., Aebersold, R., & Bähler, J. (2012). Quantitative Analysis of Fission Yeast Transcriptomes and Proteomes in Proliferating and Quiescent Cells. *Cell*, *151*(3), 671-683. https://doi.org/https://doi.org/10.1016/j.cell.2012.09.019

Marsano, R. M., & Dimitri, P. (2022). Constitutive Heterochromatin in Eukaryotic Genomes: A Mine of Transposable Elements. *Cells*, *11*(5), 761. https://www.mdpi.com/2073-4409/11/5/761

Mata, J., & Bähler, J. (2006). Global roles of Ste11p, cell type, and pheromone in the control of gene expression during early sexual differentiation in fission yeast. *Proceedings of the National Academy of Sciences*, *103*(42), 15517-15522. https://doi.org/doi:10.1073/pnas.0603403103

Matsuda, A., Asakawa, H., Haraguchi, T., & Hiraoka, Y. (2017). Spatial organization of the Schizosaccharomyces pombe genome within the nucleus. *Yeast*, *34*(2), 55-66. https://doi.org/https://doi.org/10.1002/yea.3217

McIlwraith, M. J., & West, S. C. (2008). DNA Repair Synthesis Facilitates RAD52-Mediated Second-End Capture during DSB Repair. *Molecular Cell*, *29*(4), 510-516. https://doi.org/10.1016/j.molcel.2007.11.037

Merigliano, C., & Chiolo, I. (2021). Multi-scale dynamics of heterochromatin repair. *Current Opinion in Genetics & Development*, *71*, 206-215. https://doi.org/https://doi.org/10.1016/j.gde.2021.09.007

Moreno, S., Klar, A., & Nurse, P. (1991). Molecular genetic analysis of fission yeast Schizosaccharomyces pombe. *Methods Enzymol*, *194*, 795-823. https://doi.org/10.1016/0076-6879(91)94059-l

Moser, B., Basílio, J., Gotzmann, J., Brachner, A., & Foisner, R. (2020). Comparative Interactome Analysis of Emerin, MAN1 and LEM2 Reveals a Unique Role for LEM2 in Nucleotide Excision Repair. *Cells*, *9*(2). https://doi.org/10.3390/cells9020463

Murton, H. E., Grady, P. J., Chan, T. H., Cam, H. P., & Whitehall, S. K. (2016). Restriction of Retrotransposon Mobilization in Schizosaccharomyces pombe by Transcriptional Silencing and Higher-Order Chromatin Organization. *Genetics*, *203*(4), 1669-1678. https://doi.org/10.1534/genetics.116.189118

Nagai, S., Dubrana, K., Tsai-Pflugfelder, M., Davidson, M. B., Roberts, T. M., Brown, G. W., Varela, E., Hediger, F., Gasser, S. M., & Krogan, N. J. (2008). Functional Targeting of DNA Damage to a Nuclear Pore-Associated SUMO-Dependent Ubiquitin Ligase. *Science*, *322*(5901), 597-602. https://doi.org/doi:10.1126/science.1162790

New, J. H., Sugiyama, T., Zaitseva, E., & Kowalczykowski, S. C. (1998). Rad52 protein stimulates DNA strand exchange by Rad51 and replication protein A. *Nature*, *391*(6665), 407-410. https://doi.org/10.1038/34950

Nian, L., Li, X., Li, R., & and Song-Bai, L. (2024). Types of DNA damage and research progress. *Nucleosides, Nucleotides & Nucleic Acids*, *43*(9), 881-901. https://doi.org/10.1080/15257770.2023.2277194

Noma, K., Sugiyama, T., Cam, H., Verdel, A., Zofall, M., Jia, S., Moazed, D., & Grewal, S. I. (2004). RITS acts in cis to promote RNA interference-mediated transcriptional and post-transcriptional silencing. *Nat Genet*, *36*(11), 1174-1180. https://doi.org/10.1038/ng1452

Novarina, D., Desai, R., Vaisica, J. A., Ou, J., Bellaoui, M., Brown, G. W., & Chang, M. (2020). A Genome-Wide Screen for Genes Affecting Spontaneous Direct-Repeat Recombination in Saccharomyces cerevisiae. *G3 (Bethesda)*, *10*(6), 1853-1867. https://doi.org/10.1534/g3.120.401137

Osman, F., Dixon, J., Barr, A. R., & Whitby, M. C. (2005). The F-Box DNA helicase Fbh1 prevents Rhp51-dependent recombination without mediator proteins. *Mol Cell Biol*, *25*(18), 8084-8096. https://doi.org/10.1128/mcb.25.18.8084-8096.2005

Oza, P., Jaspersen, S. L., Miele, A., Dekker, J., & Peterson, C. L. (2009). Mechanisms that regulate localization of a DNA double-strand break to the nuclear periphery. *Genes Dev*, *23*(8), 912-927. https://doi.org/10.1101/gad.1782209

Padeken, J., & Heun, P. (2014). Nucleolus and nuclear periphery: Velcro for heterochromatin. *Current Opinion in Cell Biology*, *28*, 54-60. https://doi.org/https://doi.org/10.1016/j.ceb.2014.03.001

Padeken, J., Methot, S. P., & Gasser, S. M. (2022). Establishment of H3K9-methylated heterochromatin and its functions in tissue differentiation and maintenance. *Nature Reviews Molecular Cell Biology*, *23*(9), 623-640. https://doi.org/10.1038/s41580-022-00483-w

Pai, C. C., Heitzer, E., Bertrand, S., Toumazou, S., Humphrey, T. C., & Kearsey, S. E. (2023). Using canavanine resistance to measure mutation rates in Schizosaccharomyces pombe. *PLoS One*, *18*(1), e0271016. https://doi.org/10.1371/journal.pone.0271016

Piazza, A., Bordelet, H., Dumont, A., Thierry, A., Savocco, J., Girard, F., & Koszul, R. (2021). Cohesin regulates homology search during recombinational DNA repair. *Nature Cell Biology*, *23*(11), 1176-1186. https://doi.org/10.1038/s41556-021-00783-x

Polleys, E. J., House, N. C. M., & Freudenreich, C. H. (2017). Role of recombination and replication fork restart in repeat instability. *DNA Repair*, *56*, 156-165. https://doi.org/https://doi.org/10.1016/j.dnarep.2017.06.018

Prudden, J., Evans, J. S., Hussey, S. P., Deans, B., O'Neill, P., Thacker, J., & Humphrey, T. (2003). Pathway utilization in response to a site-specific DNA double-strand break in fission yeast. *Embo j*, *22*(6), 1419-1430. https://doi.org/10.1093/emboj/cdg119

Renkawitz, J., Lademann, C. A., & Jentsch, S. (2014). Mechanisms and principles of homology search during recombination. *Nature Reviews Molecular Cell Biology*, *15*(6), 369-383. https://doi.org/10.1038/nrm3805

Rudin, N., Sugarman, E., & Haber, J. E. (1989). Genetic and physical analysis of double-strand break repair and recombination in Saccharomyces cerevisiae. *Genetics*, *122*(3), 519-534. https://doi.org/10.1093/genetics/122.3.519

Ryu, T., Spatola, B., Delabaere, L., Bowlin, K., Hopp, H., Kunitake, R., Karpen, G. H., & Chiolo, I. (2015). Heterochromatic breaks move to the nuclear periphery to continue recombinational repair. *Nature Cell Biology*, *17*(11), 1401-1411. https://doi.org/10.1038/ncb3258

Sallmyr, A., Bhandari, S. K., Naila, T., & Tomkinson, A. E. (2024). Mammalian DNA ligases; roles in maintaining genome integrity. *Journal of Molecular Biology*, *436*(1), 168276. https://doi.org/https://doi.org/10.1016/j.jmb.2023.168276

Sasanuma, H., Yamada, S., Tsuda, M., & Takeda, S. (2020). Restoration of ligatable "clean" double-strand break ends is the rate-limiting step in the rejoining of ionizing-radiation-induced DNA breakage. *DNA Repair*, *93*, 102913. https://doi.org/https://doi.org/10.1016/j.dnarep.2020.102913

Sato, A., Isaac, B., Phillips, C. M., Rillo, R., Carlton, P. M., Wynne, D. J., Kasad, R. A., & Dernburg, A. F. (2009). Cytoskeletal Forces Span the Nuclear Envelope to Coordinate Meiotic Chromosome Pairing and Synapsis. *Cell*, *139*(5), 907-919. https://doi.org/10.1016/j.cell.2009.10.039

Schipler, A., & Iliakis, G. (2013). DNA double-strand–break complexity levels and their possible contributions to the probability for error-prone processing and repair pathway choice. *Nucleic Acids Research*, *41*(16), 7589-7605. https://doi.org/10.1093/nar/gkt556

Sfeir, A., Tijsterman, M., & McVey, M. (2024). Microhomology-Mediated End Joining Chronicles: Tracing the Evolutionary Footprints of Genome Protection. *Annual Review of Cell and Developmental Biology*. https://doi.org/https://doi.org/10.1146/annurev-cellbio-111822-014426

Sharifmoghadam, M. R., Bustos-Sanmamed, P., & Valdivieso, M.-H. (2006). The fission yeast Map4 protein is a novel adhesin required for mating. *FEBS Letters*, *580*(18), 4457-4462. https://doi.org/https://doi.org/10.1016/j.febslet.2006.07.016

Smith, J., & Rothstein, R. (1999). An allele of RFA1 suppresses RAD52-dependent double-strand break repair in Saccharomyces cerevisiae. *Genetics*, *151*(2), 447-458. https://doi.org/10.1093/genetics/151.2.447

Steglich, B., Sazer, S., & Ekwall, K. (2013). Transcriptional regulation at the yeast nuclear envelope. *Nucleus*, *4*(5), 379-389. https://doi.org/10.4161/nucl.26394

Sumner, M. C., & Brickner, J. (2022). The Nuclear Pore Complex as a Transcription Regulator. *Cold Spring Harb Perspect Biol*, *14*(1). https://doi.org/10.1101/cshperspect.a039438

Swartz, R. K. R., Elisa C.; King, Megan C. (2014). A role for nuclear envelope-binding complexes in homology-directed repair. *Molecular Biology of the Cell*, *25*, 2461-2471.

Symington, L. S. (2016). Mechanism and regulation of DNA end resection in eukaryotes. *Critical Reviews in Biochemistry and Molecular Biology*, *51*(3), 195-212. https://doi.org/10.3109/10409238.2016.1172552

Torres-Rosell, J., Félix, M., & and Aragón, L. (2005). Smc5-Smc6 Complex Preserves Nucleolar Integrity in S. cerevisiae. *Cell Cycle*, *4*(7), 868-872. https://doi.org/10.4161/cc.4.7.1825

Torres-Rosell, J., Sunjevaric, I., De Piccoli, G., Sacher, M., Eckert-Boulet, N., Reid, R., Jentsch, S., Rothstein, R., Aragón, L., & Lisby, M. (2007). The Smc5–Smc6 complex and SUMO modification of Rad52 regulates recombinational repair at the ribosomal gene locus. *Nature Cell Biology*, *9*(8), 923-931. https://doi.org/10.1038/ncb1619

Triplett, M. K., Johnson, M. J., & Symington, L. S. (2024). Induction of homologous recombination by site-specific replication stress. *DNA Repair*, *142*, 103753. https://doi.org/https://doi.org/10.1016/j.dnarep.2024.103753

Truong, L. N., Li, Y., Shi, L. Z., Hwang, P. Y.-H., He, J., Wang, H., Razavian, N., Berns, M. W., & Wu, X. (2013). Microhomology-mediated End Joining and Homologous Recombination share the initial end resection step to repair DNA double-strand breaks in mammalian cells. *Proceedings of the National Academy of Sciences*, *110*(19), 7720-7725. https://doi.org/doi:10.1073/pnas.1213431110

Tsouroula, K., Furst, A., Rogier, M., Heyer, V., Maglott-Roth, A., Ferrand, A., Reina-San-Martin, B., & Soutoglou, E. (2016). Temporal and Spatial Uncoupling of DNA Double

Strand Break Repair Pathways within Mammalian Heterochromatin. *Mol Cell*, *63*(2), 293-305. https://doi.org/10.1016/j.molcel.2016.06.002

van Bueren, M. A. E., & Janssen, A. (2024). The impact of chromatin on double-strand break repair: Imaging tools and discoveries. *DNA Repair (Amst)*, *133*, 103592. https://doi.org/10.1016/j.dnarep.2023.103592

Varas, J., Graumann, K., Osman, K., Pradillo, M., Evans, D. E., Santos, J. L., & Armstrong, S. J. (2015). Absence of SUN1 and SUN2 proteins in Arabidopsis thaliana leads to a delay in meiotic progression and defects in synapsis and recombination. *The Plant Journal*, *81*(2), 329-346. https://doi.org/https://doi.org/10.1111/tpj.12730

Verstrepen, K. J., & Klis, F. M. (2006). Flocculation, adhesion and biofilm formation in yeasts. *Mol Microbiol*, *60*(1), 5-15. https://doi.org/10.1111/j.1365-2958.2006.05072.x

Vines, A. J., Cox, K., Leland, B. A., & King, M. C. (2022). Homology-directed repair involves multiple strand invasion cycles in fission yeast. *Mol Biol Cell*, *33*(4), ar30. https://doi.org/10.1091/mbc.E20-07-0433

Wang, R. W., Lee, C. S., & Haber, J. E. (2017). Position effects influencing intrachromosomal repair of a double-strand break in budding yeast. *PLoS One*, *12*(7), e0180994. https://doi.org/10.1371/journal.pone.0180994

Warmerdam, Daniël O., van den Berg, J., & Medema, René H. (2016). Breaks in the 45S rDNA Lead to Recombination-Mediated Loss of Repeats. *Cell Reports*, *14*(11), 2519-2527. https://doi.org/https://doi.org/10.1016/j.celrep.2016.02.048

Whalen, J. M., Dhingra, N., Wei, L., Zhao, X., & Freudenreich, C. H. (2020). Relocation of Collapsed Forks to the Nuclear Pore Complex Depends on Sumoylation of DNA Repair Proteins and Permits Rad51 Association. *Cell Reports*, *31*(6). https://doi.org/10.1016/j.celrep.2020.107635

Wong, X., Loo, T.-H., & Stewart, C. L. (2021). LINC complex regulation of genome organization and function. *Current Opinion in Genetics & Development*, *67*, 130-141. https://doi.org/https://doi.org/10.1016/j.gde.2020.12.007

Wright, W. D., Shah, S. S., & Heyer, W. D. (2018). Homologous recombination and the repair of DNA double-strand breaks. *J Biol Chem*, *293*(27), 10524-10535. https://doi.org/10.1074/jbc.TM118.000372

Zaratiegui, M., Vaughn, M. W., Irvine, D. V., Goto, D., Watt, S., Bähler, J., Arcangioli, B., & Martienssen, R. A. (2011). CENP-B preserves genome integrity at replication forks paused by retrotransposon LTR. *Nature*, *469*(7328), 112-115. https://doi.org/10.1038/nature09608

Zhang, J. M., Liu, X. M., Ding, Y. H., Xiong, L. Y., Ren, J. Y., Zhou, Z. X., Wang, H. T., Zhang, M. J., Yu, Y., Dong, M. Q., & Du, L. L. (2014). Fission yeast Pxd1 promotes proper DNA repair by activating Rad16XPF and inhibiting Dna2. *PLoS Biol*, *12*(9), e1001946. https://doi.org/10.1371/journal.pbio.1001946

Zhao, Y., Dominska, M., Petrova, A., Bagshaw, H., Kokoska, R. J., & Petes, T. D. (2017). Properties of Mitotic and Meiotic Recombination in the Tandemly-Repeated CUP1 Gene Cluster in the Yeast Saccharomyces cerevisiae. *Genetics*, *206*(2), 785-800. https://doi.org/10.1534/genetics.117.201285

Zhao, Y., Schreiner, S. M., Koo, P. K., Colombi, P., King, M. C., & Mochrie, S. G. (2016). Improved Determination of Subnuclear Position Enabled by Three-Dimensional Membrane Reconstruction. *Biophys J*, *111*(1), 19-24. https://doi.org/10.1016/j.bpj.2016.05.036

1